Gong *et al. Energy Mater* 2023;3:300016
DOI: 10.20517/energymater.2022.82

Energy Materials

Review

Open Access

Check for updates

Heterogeneous single-atom catalysts for energy process: recent progress, applications and challenges

Xue Gong[1], Ping Song[1], Ce Han[1], Yi Xiao[2], Xuanhao Mei[1,3], Weilin Xu[1,3,*]

[1]State Key Laboratory of Electroanalytical Chemistry, Jilin Province Key Laboratory of Low Carbon Chemical Power, Changchun Institute of Applied Chemistry, Chinese Academy of Sciences, Changchun 130022, Jilin, China.
[2]Institute for Digital Molecular Analytics and Science, Nanyang Technological University, Singapore 637457, Singapore.
[3]University of Science and Technology of China, Hefei 230026, Anhui, China.

***Correspondence to:** Prof. Weilin Xu, State Key Laboratory of Electroanalytical Chemistry, Jilin Province Key Laboratory of Low Carbon Chemical Power, Changchun Institute of Applied Chemistry, Chinese Academy of Sciences, 5625 Renmin Street, Changchun 130022, Jilin, China. E-mail: weilinxu@ciac.ac.cn

How to cite this article: Gong X, Song P, Han C, Xiao Y, Mei X, Xu W. Heterogeneous single-atom catalysts for energy process: recent progress, applications and challenges. *Energy Mater* 2023;3:300016. https://dx.doi.org/10.20517/energymater.2022.82

Received: 25 Nov 2022 **First Decision:** 18 Jan 2023 **Revised:** 7 Feb 2023 **Accepted:** 3 Mar 2023 **Published:** 7 Apr 2023

Academic Editors: Hao Liu, Yuping Wu, Bin Wang **Copy Editor:** Fangling Lan **Production Editor:** Fangling Lan

Abstract

Single-atom catalysts (SACs) with high activity, unique selectivity, and nearly 100% atom utilization efficiency are promising for broad applications in many fields. This review aims to provide a summary of the current development of SACs and point out their challenges and opportunities for commercial applications in the energy process. The discussion starts with an introduction of various types of SACs materials, followed by typical SACs synthetic methods with concrete examples and commonly used characterization methods. The state-of-the-art synthesis methods, whereby SACs with stabilized single metal atoms on the substrate without migration and agglomeration could be obtained, are emphasized. Next, we give an overview of different types of substrates and discuss the effects of substrate species on the structure and properties of SACs. Then we highlight the typical applications of SACs and the remaining challenges. Finally, a perspective on the opportunities for the development of SACs for future commercial applications is provided.

Keywords: Single-atom catalysts, synthesis method, substrates, structure and properties, applications

© The Author(s) 2023. **Open Access** This article is licensed under a Creative Commons Attribution 4.0 International License (https://creativecommons.org/licenses/by/4.0/), which permits unrestricted use, sharing, adaptation, distribution and reproduction in any medium or format, for any purpose, even commercially, as long as you give appropriate credit to the original author(s) and the source, provide a link to the Creative Commons license, and indicate if changes were made.

INTRODUCTION

Heterogeneously supported noble metal catalysts have been extensively used in the industry community due to the advantages of being economical, having favorable activity for many chemical reactions, and being energy-saving[1-5]. Highly efficient catalysts are urgently required as more than 80% of globally produced chemicals include catalytic processes[6]. In spite of this, the scarcity and high costs of noble metals place great restrictions on the sustainable development of the corresponding energy process. The improvement of catalytic efficiency, the reduction of noble metal loadings on catalysts, and the development of candidates based on earth-abundant non-noble metals are important issues for the development of renewable energy technologies in the future.

Downsizing metal particles or clusters to the atomic level with atomically isolated active sites is a straightforward method to increase metal utilization efficiency. This concept was realized by Qiao *et al.* in 2011[7]. In principle, SACs provide 100% metal atom dispersion on an appropriate substrate, in which isolated metal atoms are anchored by surrounding coordination species against migration and aggregation into large particles. Thus, the SACs usually possess unique electronic structures as a result of strong interaction between the metal atom and substrate, making SCAs exhibit excellent catalyst activity, selectivity, and economic benefit in multiple catalytic fields in contrast with traditional nanocatalysts[8-10]. Besides, a SAC is a good model catalyst for investigating its structure-activity relationship owing to its atomic dispersion of the active components. Benefiting from the above advantages, SACs have received much attention in the energy-related catalytic process.

The SACs have been applied extensively in all kinds of energy fields, such as O_2 reduction reaction[11,12], CO_2 reduction reaction[13,14], N_2 reduction reaction[15,16], H_2 evolution reaction[17], CH_4 conversion reaction[18], and so on. As discussed detailedly in this review, compared to metal particle counterparts, the SACs provide many unique catalytic performances, such as outstanding activity, improved selectivity, better durability, and resistance to CO or methanol poisoning. To date, most of the reported works on SACs have been related to exploring universal synthesis methods to improve the metal loadings of single metal atoms and scale-up technology, making SACs more suitable for industrial applications. However, there are still some challenges for SACs. One of them is the aggregation of metal atoms as a result of the large high atom surface energy, which leads to low metal loading and further loss of catalytic performance. Besides that, many in-situ experiments have shown that the structures of SCAs materials can go through remarkable changes in the real reaction processes. Thus, in a certain catalytic reaction, whether the single atoms on the substrate are stable enough to stay well dispersed is also a hot issue.

In this review, we focus on the recently proposed synthesis methods of SACs. Additionally, we highlight and summarize the advanced synthesis strategies and substrates for SACs accompanied by enhanced properties and stability, stressing the mechanism of how the SACs stay well dispersed and stable during the synthesis and reaction processes. Then, we discuss the possible factors that affect the properties and stabilities. Furthermore, we summarize the typical applications of SACs and the corresponding mechanistic studies to illustrate the structure-property relationship. We also provide a brief overview of the current challenge of high-density SACs fabrication and scale-up technology. Finally, we propose an outlook for the future and potential development direction of SACs.

SYNTHETIC METHODS FOR SACS

The synthesis method for SACs is generally unique from metal particle-based catalysts, as it is well established that the surface free energy of metal increases with downsizing the metal particle, which leads to the aggregation of single atoms into clusters or nanoparticles. The key point is to realize the atomic

dispersion of the target metal against agglomeration into particles, so it is usually necessary to create strong interaction between single metal atoms and the corresponding substrate. Here we summarize some synthesis strategies of SACs reported recently.

Wet-chemistry method

Wet-chemistry methods are frequently used because of their low cost, simple synthesis process, and easy scale-up. The key point for wet chemistry approaches is confining the location of the introduced metal active sites on the substrate to prevent their aggregation into particles[19]. The wet-chemistry method is usually composed of two steps[20]: (1) mixing of the metal precursor and substrate; and (2) reduction or oxidation treatment to activate the catalyst. For example, Yang *et al.* reported a universal synthesis route by complexing metal cations with 1,10-phenanthroline, adsorbing the obtained complexes onto carbon black, followed by heat treatment of the surface-modified carbons at 600 °C under an inert gas atmosphere [Figure 1A][21]. This method can be applied to synthesize a library of carbon black supported SACs (e.g., Ni, Mn, Fe, Co, Cr, Cu, Zn, Ru, and Pt). In order to further restrict the movement of mononuclear metal precursors both in the pretreatment step and activation step, some researchers proposed an ice-assisted adsorption strategy combined with a photochemical reduction step, as shown in Figure 1B[22-24]. For a Pt SAC, typically, its synthesis includes the following steps: Firstly, the Pt precursor aqueous solution is frozen with liquid nitrogen; then, the ice is treated by UV irradiation to reduce the metal precursors into individual metal atoms. After that, the obtained Pt single-atom solution is mixed with different substrate dispersions to obtain Pt SACs on different supports[22]. However, there was a limitation on controlling the single isolated atom on the substrate; usually, the loading of single atoms was below 7.5 wt.%[25]. Moreover, a wet chemistry method is usually a trial-and-error process. The limitations of this approach include the difficulty of accurately controlling the location of the target active sites on the support surface.

Pyrolysis

Up to now, most reported SACs usually require a high-temperature pyrolysis step (usually 700-1,100 °C) to obtain a highly stable single-atom active structure. The process is simple, and usually, no post-processing is required. Nevertheless, the rigorous pyrolysis treatment always causes noble metals of ultrasmall size (single atoms or clusters) to inevitably aggregate into large particles as a result of high surface free energy. This phenomenon is usually known as thermal deactivation or sintering, which may reduce the active surface of metal and catalyst reactivity[26-28]. To overcome this difficulty, the pyrolysis procedure is usually combined with some other strategies (such as spatial confinement, coordination with heteroatoms, and defect anchor strategies) to construct strong interactions between central metal single atoms and substrate[29-33]. In the spatial confinement process, porous materials with unique pore sizes and structures usually act as hosts to trap mononuclear metal precursors, which can prevent metal aggregation during the high-temperature pyrolysis procedure. Xiong *et al.* used a zeolitic imidazolate framework to encapsulate the Rh precursor [$Rh(acac)_3$], followed by a 900 °C pyrolysis reduction treatment[34]. It is an effective method to disperse and immobilize an Rh single atom since the size of $Rh(acac)_3$ is between the large cavities and small pores of ZIF-8. And a strong interaction between Rh and the substrate was formed, ensuring the good dispersion of Rh atomic species. To stabilize single metal atoms during the high-temperature pyrolysis procedure, some researchers applied heteroatoms (N, P, S, *etc.*) to anchor single metal atoms[6]. Chen *et al.* proposed Fe SACs with single iron atomic sites supported on an N, P, and S co-doped carbon framework by high-temperature pyrolysis combined with a heteroatom coordination strategy; the preparation process is shown in Figure 2A[33]. During the pyrolysis, N, P, and S were co-doped, in which S and P atoms regulate the electronic structure of the Fe-N_4 active site, leading to excellent oxygen reduction reaction (ORR) performance for these Fe SACs both in acidic and alkaline conditions. Meanwhile, defect engineering is also a powerful technology to stabilize single atoms via strong electro-transfer interactions between metal atoms and substrate. Because of the defect-rich surface (usually surface oxygen vacancies) and strong interaction

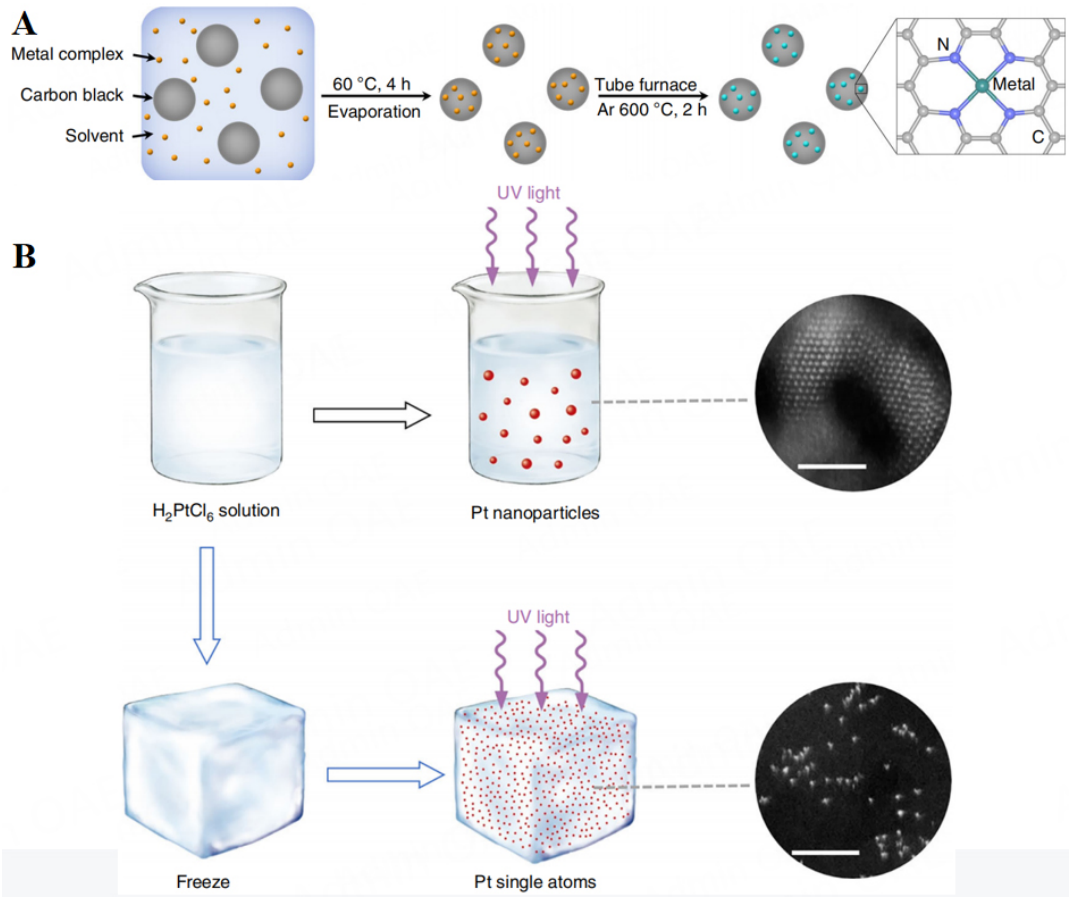

Figure 1. (A) The universal synthesis procedure. Metal single-atom catalysts (M-SACs) are prepared in two steps. Reproduced from Ref.[21] with permission from Springer Nature. (B) Schematic illustration of the iced-photochemical process. Reproduced from Ref.[22] with permission from Springer Nature.

with a metal atom, metal oxides have been used as effective catalyst supports[35-38]. Besides, creating carbon defects on the carbon-based substrate is also an effective method to prepare SACs. Liu *et al.* created an abundance of carbon defects by treating cost-effective carbon black hydrothermally (200 °C) in a sealed ethanol solution containing a certain amount of H_2O_2[39]. Then the obtained defective carbon was used as a substrate to absorb $Pt(acac)_2$, followed by pyrolysis at 900 °C under an argon atmosphere. The well-dispersed Pt SACs were successfully synthesized. Moreover, the obtained Pt SACs showed remarkable ORR performance, as shown in Figure 2B-D. However, because of the limitation of defects density and the drawback of high-temperature pyrolysis, it is hard to fabricate SACs with high metal loading.

Electrochemical deposition method

Electrochemical deposition is an effective strategy for the synthesis of SACs, as the bulk metal can be dissolved into a solution and anchored by the support[40-44]. Tavakkoli *et al.* developed a facile electroplating method by reducing the electroplating time and achieving single nanotubes (SWNTs) that supported pseudo-atomic-scale dispersion of Pt (individual atoms or subnanometer clusters) [Figure 3A and B][45]. And this kind of catalyst material has an ultralow Pt loading as well as extraordinary electrocatalytic activities for the HER. Motivated by the breakthrough, Zhang *et al.* proposed a potential-cycling method with a three-electrode cell in neutral media (pH = 7.2) to synthesize Pt SACs, in which large areas of isolated Pt single atoms were grown on Ni foam *in situ*, as shown in Figure 3C[46]. These SACs can be directly used

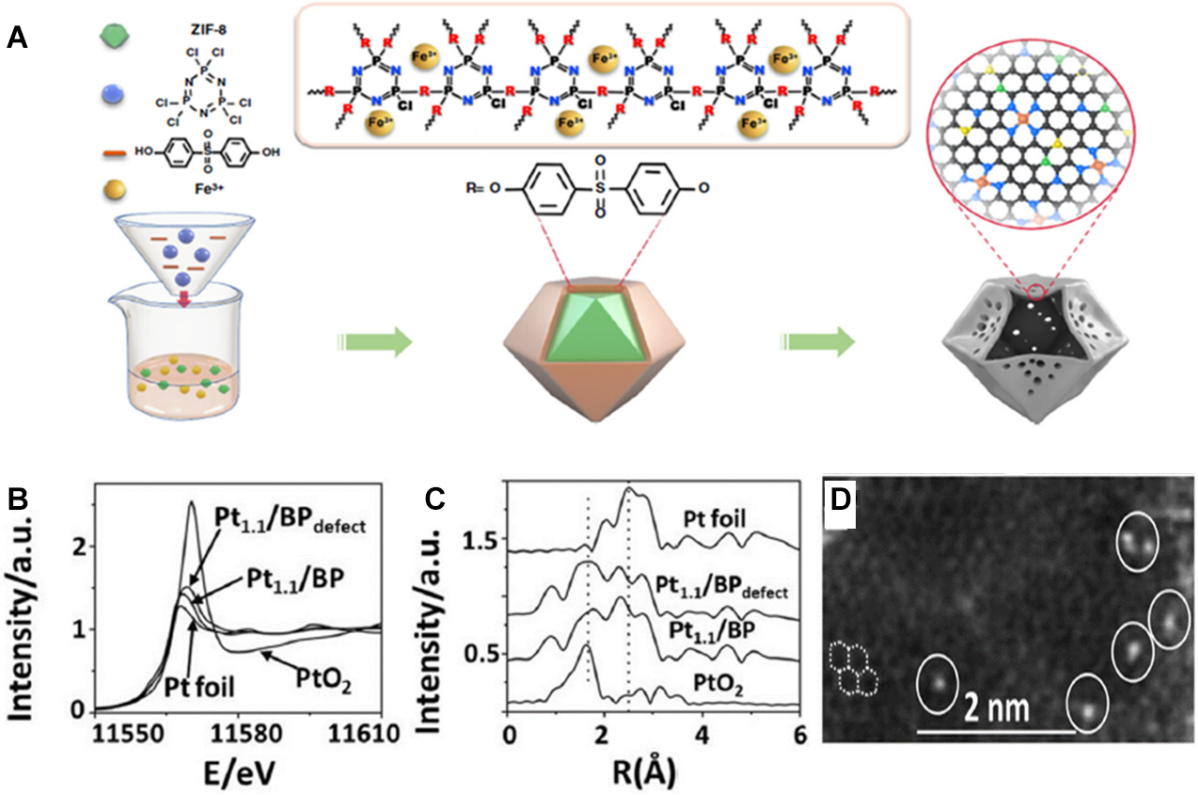

Figure 2. (A) Illustration of the preparation process of single iron atomic sites supported on nitrogen, phosphorus, and sulfur co-doped hollow carbon polyhedron (Fe-SAs/NPS-HC) by pyrolysis combined with a heteroatom doping strategy; Reproduced from Ref.[33] with permission from Springer Nature. Electrochemical and physical characterization of different catalysts. (B) Pt L_3-edge XANES for Pt SACs and corresponding Pt foil, PtO_2; (C) The k^2-weighted R-space FT spectra from EXAFS for Pt SACs and corresponding Pt foil, PtO_2; (D) High-angle annular dark field scanning transmission electron microscope (HAADF-STEM) image to show the distribution of Pt atoms on carbon defects. Reproduced from Ref.[39] with permission from Wiley-VCH.

for HER electrocatalysis without binders and possess an outstanding HER property comparable to commercial Pt/C. Furthermore, a general electrochemical deposition strategy was proposed, and more than 30 kinds of SACs were successfully obtained from cathodic or anodic deposition by controlling the variety of metal precursors and substrates. The electrochemical deposition mechanism is shown in Figure 3D-F, in which cations were driven towards the cathode by the applied electric field and deposited on the supports for the cathode deposition, while for the anodic deposition, anions were driven by the applied electric field towards the anode. The drawbacks of the electrochemical deposition method are that there exists an upper limit to mass loading (usually less than 4.7 wt.%) and that it is related to the level of supersaturation on the substrate[47]. When the loading of metal surpasses the limitation, the isolated metal atoms tend to aggregate into clusters or form multilayer structures with nonuniform coverage.

Chemical etching

Chemical etching is also an effective strategy for obtaining SACs with relatively high metal loading, although the synthesis route is usually complicated[48-50]. For example, Qiu synthesized Ni SACs supported by nanoporous graphene, and the fabrication process is shown in Figure 4A[51]. Firstly, nanoporous Ni substrates were prepared by dealloying NiMn alloy sheets, and then one atomically thick graphene layer was grown on the nanoporous Ni surface by the chemical vapor deposition method, followed by the key step of etching the Ni metals to generate the isolated atomic Ni single atoms on the stable graphene substrate in 2.0 M HCl solution. Finally, free-standing graphene-supported Ni SACs were obtained by controlling the

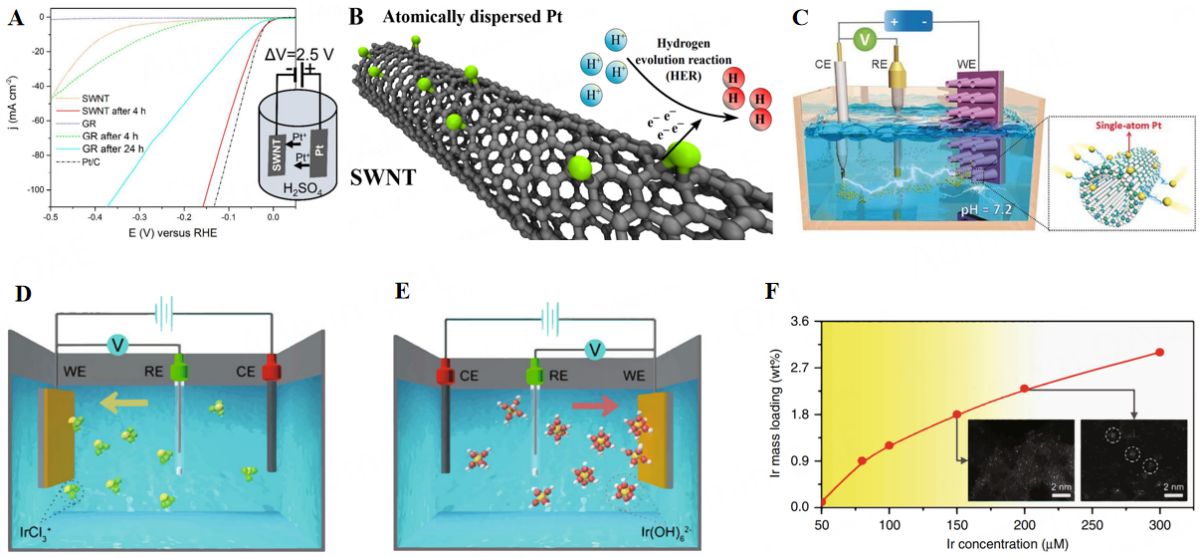

Figure 3. (A) Polarization curves of the SWNT (orange), the SWNT activated for 4 h (red), GR (blue), GR activated for 4 h (green) and 16 h (cyan), and Pt/C (black). (B) Structure diagram of the SWNT with isolated, dispersed Pt; reproduced from Ref.[45] with permission from the American Chemical Society. (C) Schematic diagram of the potential-cycling synthesis method process. Reproduced from Ref.[46] with permission from Wiley-VCH. Schematic of cathodic (D) and anodic (E) deposition of Ir species; The yellow, green, red, and white spheres represent Ir, Cl, O, and H atoms, respectively. Ir mass loadings as a function of Ir concentration in the 1 M KOH electrolyte for anodic (F) deposition. The scanning cycle number was kept at ten for cathodic deposition and three for anodic deposition. The inset images correspond to the HAADF-STEM images of the samples obtained at a certain concentration. The areas in white circles indicate the agglomerations of single atoms to form clusters. Reproduced from Ref.[47] with permission from Springer Nature.

etching time. The catalyst showed a very low overpotential (around 50 mV) for HER and remarkable stability compared with Pt and reduced graphene oxide. Wang *et al.* used Fe_3O_4 nanocubes as the template and sources of Fe to synthesize Fe SACs by the method of *in situ* ligand carbonization to form superlattices, followed by acid etching and NH_3 activation, as shown in Figure 4B[52]. The obtained Fe SACs with well-dispersed Fe atoms supported on the carbon framework substrate [Figure 4C] showed outstanding ORR properties in alkaline media and comparable zinc-air battery performance comparable to commercial Pt/C catalysts. Recently, Li *et al.* modified the normal chemical etching method by selectively removing unneeded metallic materials realizing the accurate match between the bond energies of metal-metal/metal-substrate and the strength of the etching agent[53]. Specifically, excessive Pd was loaded on the PCN substrate first, and then an appropriate etching reagent was selected as chemical scissors to selectively cut the Pd-Pd metal bonds and keep the Pd-PCN bonds, achieving 2.02 wt.% loading of isolated single Pd atoms on substrates. The scheme for the chemical scissors procedure is shown in Figure 4D-L; typically, Pd-Pd bonds are selectively broken by Fe^{3+} while keeping the Pd-PCN bonds as a result of the stronger interaction between Pd and PCN. And the obtained Pd-based SACs show outstanding catalytic activity in photocatalytic CO_2 reduction with CH_3OH generation of 597.8 ± 144.6 μmol h^{-1} g^{-1} and selectivity of 81.3 ± 3.8%. Template support is usually required, such as metal templates or SiO_2 support. And it is hard to control the degree of etching to obtain the designed architecture.

Photochemical method

A photochemical reduction strategy can be used to prepare SACs with relatively high metal loading with the advantages of fast reaction, room temperature operation, and easy scale-up[23,54-58]. And this method usually needs to be combined with another strategy to stabilize single metal atoms. Liu *et al.* reported a stable Pd_1/TiO_2 catalyst material using the photochemical method[55]. Ultraviolet (UV) light was adopted to induce the

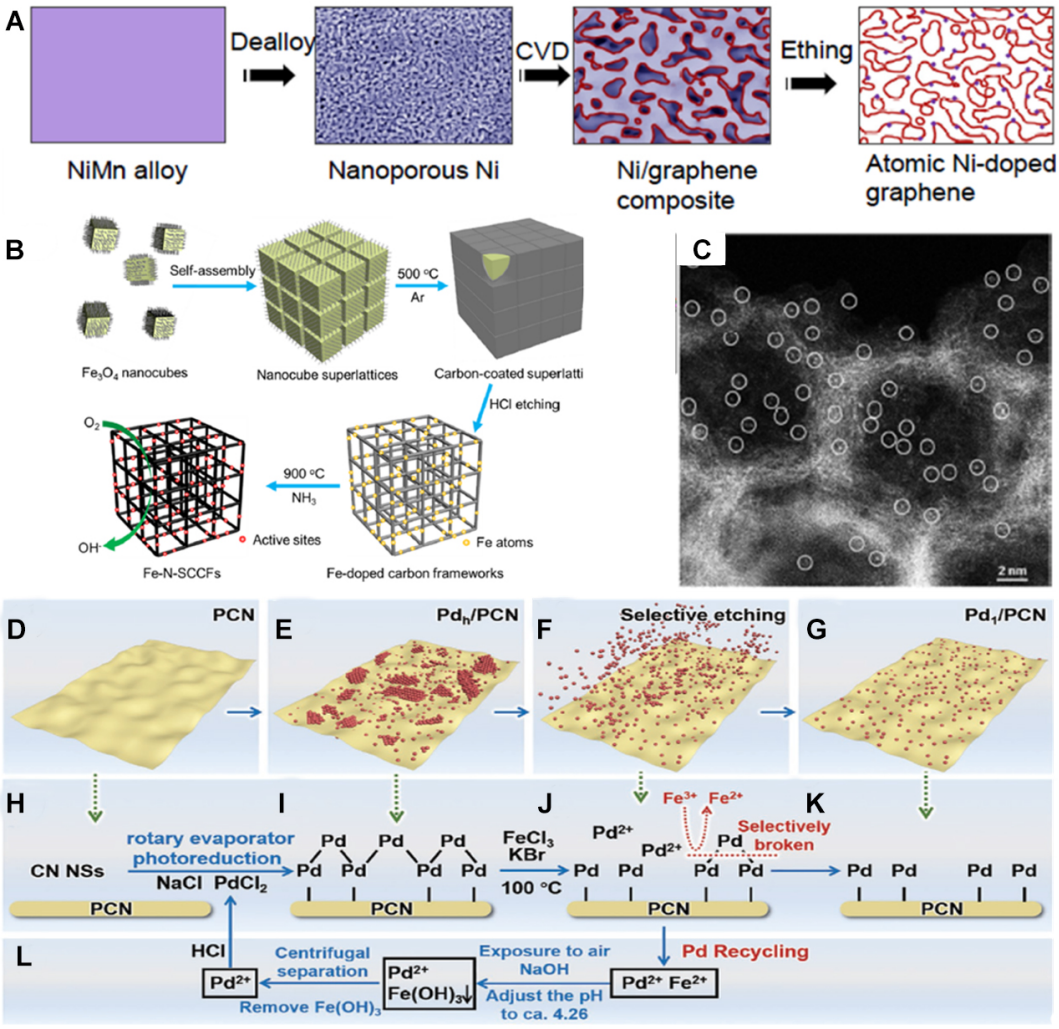

Figure 4. (A) Schematic illustration of the fabrication process of Ni-doped nanoporous graphene; Reproduced from Ref.[51] with permission from Wiley-VCH. (B) Schematic illustration of the fabrication of Fe SACs; (C) Enlarged HAADF-STEM image of Fe-N-SCCFs. Reproduced from Ref.[52] with permission from the American Chemical Society. Scheme for the construction of high-loading single-atom Pd1/PCN with chemical scissors. (D and H) The models of PCN, (E and I) The models of Pdh/PCN, (F and J) The schemes of selective etching; (G and K) As-synthesized Pd1/PCN. Only bonds between Pd and PCN have remained. (L) Recycling Pd to avoid waste. Reproduced from Ref.[53] with permission from Wiley-VCH.

formation of ethylene glycolate radicals on TiO_2 nanosheets, which is the key step to removing Cl^- from Pd atoms and stable isolated Pd atoms by forming abundant Pd-O bonds. The TEM images and X-ray diffraction pattern results showed that no Pd nanoparticles were generated during the UV treatment process. Furthermore, Ge *et al.* proposed an *in situ* photocatalytic reduction route combined with a freezing strategy[23]. Firstly, the mixture solution of K_2PdCl_4 and TiO_2 nanoparticles was frozen to the ice with the help of liquid nitrogen. Next, irradiation of the ice with Xe light, which can excite TiO_2 to generate photogenerated electrons, subsequently facilitated the reduction of Pd precursors ($PdCl_4^{2-}$) to obtain Pd_1/TiO_2 SACs. Well-dispersed Pd single atoms were observed. As expected, the Pd_1/TiO_2 SACs showed remarkably enhanced HER activity with an H_2 production rate around 10 mol $g^{-1}h^{-1}$ higher than that of the Pd nanoparticles/TiO_2 catalyst material (1.95 mol $g^{-1}h^{-1}$). Isolated dispersed metal single atoms and clusters may co-exist even at a low metal loading when directly treating the mixture of metal precursor and substrate proved by Lu, as shown in Figure 5[58]. Pd $_{SA+C}$/SAPO-31 with Pd loading of 0.38 wt.% was synthesized by

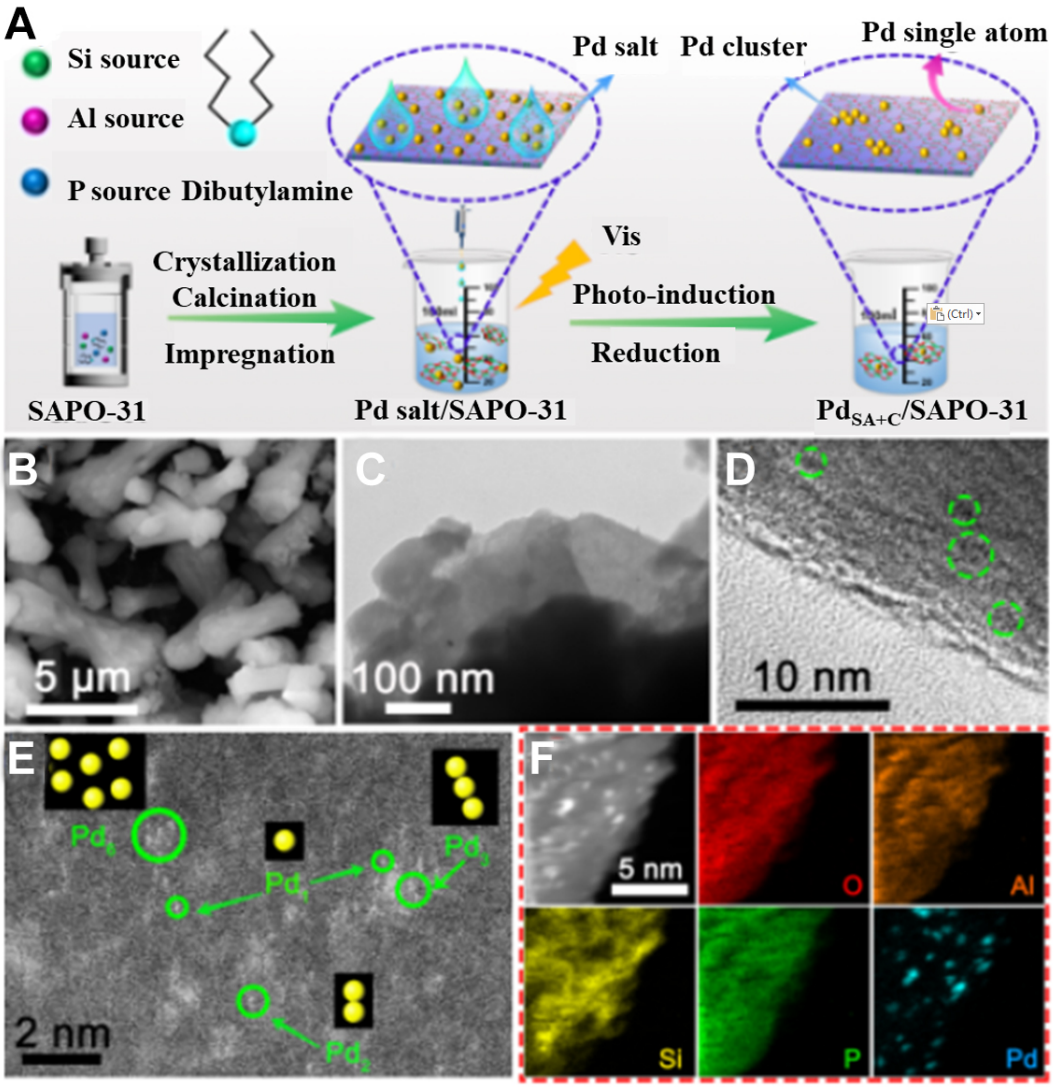

Figure 5. Schematic illustration for the construction and characterization of Pd_{SA+C}/SAPO-31. (A) Synthetic route. (B) SEM, (C) TEM, (D) HR-TEM and (E) AC HAADF-STEM images. (F) STEM-EDS elemental mapping. Reproduced from Ref.[58] with permission from Springer.

photoinduction UV treatment. The drawback of this route is that using ultraviolet is not environmentally friendly. Additionally, it is difficult to obtain ultra-high metal loading(> 10 wt.%) SACs due to the limitation of controlling single atom structure during the process. Furthermore, it is worth noting that the photochemical reduction strategy is used more to synthesize precious metal catalysts.

Atomic layer deposition method

Atomic layer Deposition (ALD) is a powerful technology to synthesize SACs material with atomically precise control. Additionally, due to its self-limiting gas-surface reaction nature, ALD has the advantages of accurately controlling the layer thickness at the angstrom level, surface chemical selectivity, and being suitable for a porous substrate[59-63]. Fabrication of SACs by the ALD method usually contains two main steps, as shown in Figure 6A and B[64]. Taking Pt_1/graphene SACs as an example, firstly, the Pt precursor reacted with the oxygen species on the substrate. Next, the precursor ligands were changed to Pt-O by an oxygen pulse. The Pt SACs catalyst can be synthesized with atomically precise design and control by

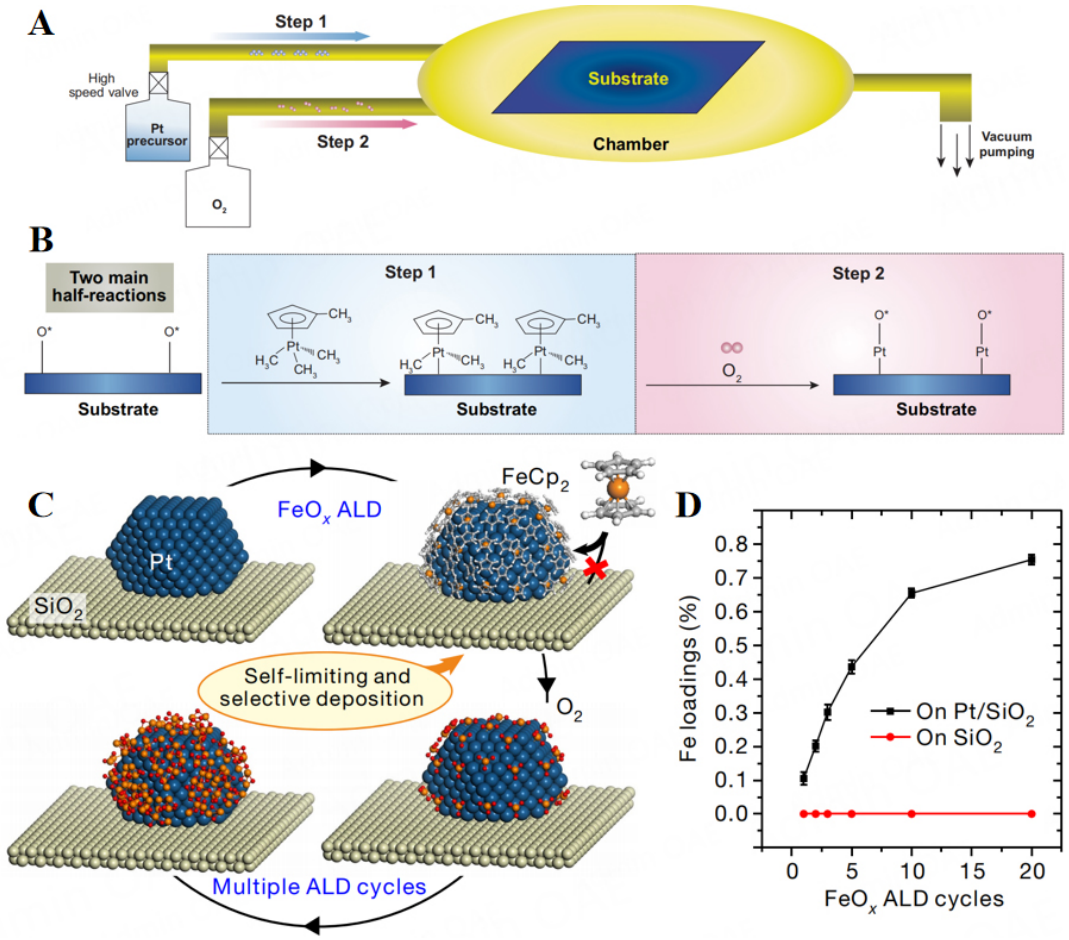

Figure 6. (A) Schematic illustrations of the deposition of single-atomic Pt on substrates through the ALD method. (B) The detailed two main half reactions during a whole ALD cycle. Reproduced from Ref.[64] with permission from Oxford University Press. (C) Schematic illustration of low-temperature selective FeO_x ALD on a Pt/SiO_2 catalyst to form isolated FeO_x on Pt nanoparticles; (D) Fe loadings in the *x*cFe-Pt/SiO_2 and *x*cFe/SiO_2 samples; Reproduced from Ref.[65] with permission from Springer Nature.

changing the ALD operation parameter. Cao *et al.* reported an atomically dispersed $Fe_1(OH)_x$ on Pt nanoparticles by ALD strategy, as shown in Figure 6C[65]. FeO_x was selectively deposited on Pt nanoparticles by the ALD process by exposing the sample to $FeCp_2$ and O_2 at a relatively low temperature alternately. Then the coverage of FeO_x on Pt nanoparticles was precisely controlled by adjusting the number of ALD cycles, as shown in Figure 6D. The obtained Fe SACs with atomically dispersed iron hydroxide deposited on silica-supported platinum nanoparticles showed remarkable activity of preferential oxidation of CO in hydrogen, achieving 100% CO conversion at a temperature range of 198 K to 380 K. Wang *et al.* proposed a general ALD method to deposit isolated Fe atoms on various substrates with a maximum Fe loading of up to 1.78 wt.%[66]. The ferrocene and hydrogen were used as precursors, and a fluidized bed as a reactor. During the ALD process, Fe single atoms on the different substrates were obtained by optimizing the parameters, including the dose time of ferrocene and the number of ALD cycles. XAS results and HAADF-STEM images confirmed the good dispersion of Fe atoms. The Fe/SiO_2 SACs showed a high level of catalyst activity in the CO oxidation reaction, which is more than 2 orders of magnitude higher than that of other reported iron oxide catalysts. The long-term stability test indicated that the Fe/SiO_2 catalyst was still active and durable even under harsh conditions.

Other strategies

Besides the mentioned SACs synthesis method above, many other strategies have been developed to prepare SACs. The central core is to restrict the diffusion and aggregation of metal precursors both in the solution phase and reduction process, for example, using microwave-assisted strategies[67] and ionic-liquid-assisted methods[68]. It is still a big challenge to realize the outstanding performance and precise control of the SACs structure.

TYPICAL CHARACTERIZATION METHODS OF SACS

To confirm the successful synthesize of SACs and characterize the environments of singles atoms are necessary. Up to now, several specific methods have been adopted for studying the structure of SACs, including X-ray photoelectron spectroscopy (XPS)[69], high-angle annular dark-field scanning transmission electron microscopy (HAADF-STEM)[70-72], energy-dispersive X-ray spectroscopy (EDX)[73,74], high resolution scanning tunneling microscopy (STM)[69,75,76], electron energy loss spectroscopy (EELS)[77-79], X-ray absorption spectroscopy(XAS)[80-82], surface-enhanced Raman spectroscopy(SERS)[83,84], and Fourier-transform infrared (FTIR)[85-87] spectroscopy. XPS usually be adopted to give information on the electronic state and composition on the surface of a sample since the structure and electronic state of active single-atom metal in SCAs are usually different from corresponding metal particles or metal oxide counterparts. However, XPS must combine with other characterization techniques to reach an accurate conclusion. HAADF-STEM is a useful method to characterize the dispersion state of a single metal atom directly. It usually combines with the EDX approach, which can be used to confirm the distribution of the elements. However, HAADF-STEM can only give information on selected areas. In contrast, STM is another kind of advanced microscopy technique to characterize the distribution of single metal atoms on catalyst surface, which can be applied to many working conditions, such as ultra-high vacuum, the gaseous or liquid atmosphere at a wide temperature range. EELS is conducted on TEM or STEM, which is usually used to identify single atoms by providing information on chemical composition, stoichiometry, energy levels, and electronic structure of catalysts. XAS is a powerful technique that has been applied to characterize the electron structure and chemical environment of SACs, including the X-ray absorption fine structure (XANES) and the extended X-ray absorption fine structure (EXAFS). It can provide rich chemical environmental information, such as electron and oxidation states, chemical binding information, the interatomic distance, and the coordination number of specified elements. It is one of the most straightforward and usual approaches to confirm the successful synthesis of SACs. Besides, SERS was also adopted to investigate single atoms on catalysts since different chemical states cause obviously different Raman shifts. However, the SERS can only be applied to some special metal systems, which is not suitable for most SACs. Furthermore, FTIR is used to characterize the structure of SACs molecules, which usually requires probe molecules to combine with specific metal atoms. So FTIR can be used to determine the dispersion state of typical species due to the limitation of the type of probe molecules. With the development of SACs, more and more useful characterization techniques will be explored to confirm the structure of SACs.

OVERVIEW OF SUBSTRATES FOR SACS

Interactions between active metal and substrate play an important role in stabilizing isolated single metal atoms during the synthesis process and influencing the catalytic performance and stability. The substrates must meet some special requirements for different applications. Good conductivity and corrosion resistance of the substrate are needed for electrocatalysis, and good stability at high temperatures is required for thermocatalysis. The typical light-harvesting capacity is essential for photocatalysis. This part summarized the recently most used substrate for SACs and discussed the relationship between structure and performance.

Metal oxide

The metal oxide was used as a substrate for many SACs due to its particular properties, such as abundant anchor sites (steps, corners, vacancies, functional group), special surface acidity or basicity, and redox features[19]. The strong interaction between the metal site and the metal oxide substrate may influence the catalytic performance as a result of synergistic effects. The commonly used metal oxide substrate includes FeO_x[88-90], CeO_2[91-93], TiO_2[94-97], MnO_2[98-100], CoO_x[101-103], NiO[104], CuO[105,106] and ZnO[107]. Marcinkowski *et al.* developed Pd SACs with $Fe_3O_4(001)$ as substrate and investigated the effect of annealing on the $Pd/Fe_3O_4(001)$[89]. As shown in Figure 7A-C, Pd exists only as single atoms at room temperature and tends to aggregate into clusters when heating the surface to 550 K. And this type of SACs significantly lowers the barrier to the oxidation of methanol. Liu reported a kind of Ru SACs with isolated Ru single atoms on metal oxide ($MgAl_{1.2}Fe_{0.8}O_4$, MAFO)[90]. They fabricated the Ru/MAFO SACs directly from RuO_2 material by heating the mixture of RuO_2 and strongly interacting substrate. They proved that strong covalent metal-support interaction between active metal and metal oxides promotes the transformation of RuO_2 to Ru single atoms. The obtained Ru SAC shows remarkable thermal stability and enhanced activity for N_2O decomposition. Yu *et al.* construct stable Cu SACs with coordination-unsaturated and atomically dispersed Cu species in a sintered Cu-Ce catalyst[108]. The XANS results (as shown in Figure 7D-I) confirmed that the Cu sites were atomically dispersed on ceria in the form of CuO_X and Cu-[O]-Ce, verifying the presence of a strong interaction between copper and substrate (CeOx). And the resulting Cu SACs showed outstanding activity in catalyzing CO oxidation with a CO consumption rate of 6,100 μmol $CO{\cdot}gCu^{-1}{\cdot}s^{-1}$ at 120 °C, around 20 times as compared to other reported Cu-based catalyst material. Additionally, this catalyst possessed good cyclic stability even under harsh conditions. Moreover, it is worth noting that the coordination environment of the active metal sites may be altered by the synthesis conditions and covalent metal-support interaction; even on the same kind of oxide substrate, the electronic state of the single-atom metal is hard to be the same.

Graphene

Graphene has been proven to be a superior substrate for SACs as a result of its unique structure and electronic properties. There are abundant anchor sites for single-atom metal on pristine graphene surfaces and mainly including three types as shown in Figure 8A: (1) the top site where active metal sits above a carbon atom; (2) the hollow site (H site) where active metal locates above the center of the hexagonal ring; (3) the bridge site (B site) where active metal coordinates to the C-C bond[109]. The graphene-based SACs usually have superb stability as a result of strong ionic bonding and covalent bonding between metal atoms and graphene. Zhang *et al.* obtained atomically dispersed Ru on N-doped graphene by dispersing the graphene oxide (GO) in deionized water, sorption of Ru precursor $[Ru(NH_3)_6Cl_3)]$ and high-temperature pyrolysis at NH_3 atmosphere[110]. The GO may possess strong interaction with metal and high sorption capacity due to its abundant oxygen-containing functional groups. HAADF-STEM proved that isolated Ru single atoms were well dispersed on the surface of N-doped GO. And electrochemical measurement results showed that this kind of Ru SACs with N-doped graphene performs a high ORR activity in acidic conditions and durability as well as tolerance against CO poisoning. Density functional theory (DFT) calculation indicated that the active center was Ru-oxo-N_4. Tsounis *et al.* synthesized Pt SACs with isolated Pt single atoms anchored at the edges of edge-rich vertically aligned graphene, and the details are shown in Figure 8B-E[111]. Firstly, vertical graphene was grown on carbon fiber paper. Then the edge density of GO was increased by Ar plasma treatment. Subsequently, the Pt was partially reduced by the local redox environment created by the graphene edges (electroless deposition) with H_2PtCl_6 as Pt resource. The results of XAS and DFT calculation indicated that there was a strong interaction between the graphene edge and Pt SACs with modified GO as a substrate. Compared to the catalysts with Pt atoms coordinated in mixed environments, the enhanced performance can be obtained when applied the Pt SACs to HER in alkaline conditions.

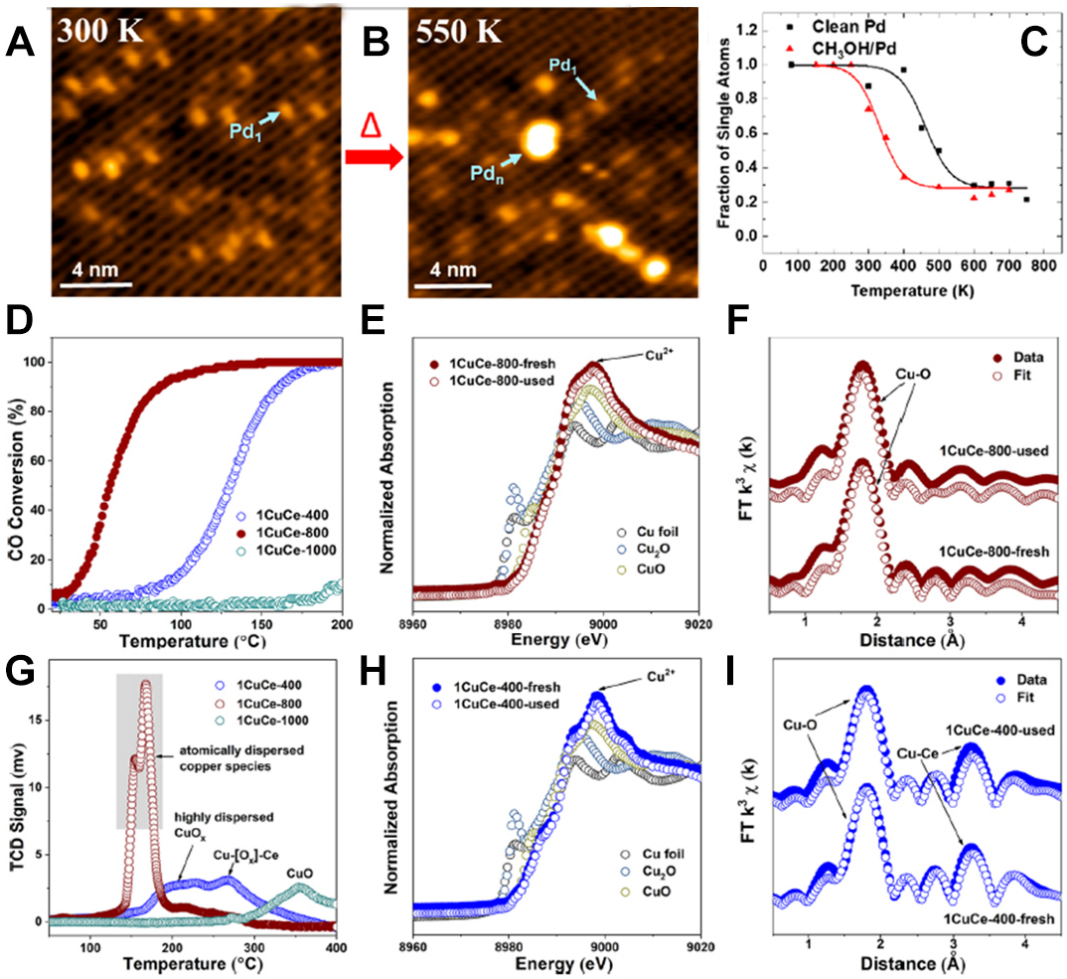

Figure 7. Examination of Pd sintering as a function of annealing temperature. (A) STM image of 0.1 Pd atoms/u.c. at room temperature compared to (B) the same surface after heating to 550 K. (C) XPS Pd $3d_{5/2}$ data showing the fraction amount of Pd single atoms for surfaces with 0.1 Pd atoms/u.c. for a surface free of adsorbates (black points) and a surface covered with methanol/ methoxy (red points). Reproduced from Ref.[89] with permission from the American Chemical Society. (D) Light-off test of CO oxidation ([CO] = 1%, $[O_2]$ = 20% and balanced with N_2 at a GHSV of 80,400 mL·gcat^{-1}·h^{-1}), (E) H_2-TPR rofiles over 1CuCe catalysts with different calcination temperatures. XANES spectra of (F) 1CuCe-800 and (G) 1CuCe-400. Extended x-ray absorption fine structure (EXAFS) spectra of (H) CuCe-800 and (I) 1CuCe-400. Reproduced from Ref.[108] with permission from the American Chemical Society.

MOF/ZIF

Metal-organic frameworks (MOFs) have been widely used as substrates for SACs because the MOF is a perfect platform for stabilizing desired metal species. Meanwhile, benefiting from the ultrahigh surface areas, well-defined pore structure, and flexible tunability, MOFs have unique advantages in energy-related aspects[1,112,113]. Therefore, sharp attention has been paid to the development of MOF-derived SACs. It has been confirmed that the single-metal active site can be located on the metal nodes, organic linkers, or encapsulated into MOF. Jiao *et al.* synthesized a single-atom iron-implanted N-doped porous carbon using a novel MOF-based mixed ligand strategy[114]. As shown in Figure 9A, the Fe-TCPP and H_2-TCPP were chosen as representative precursors, affording a series of isostructural MOFs. Upon pyrolysis and subsequent ZrO_2 removal, Fe-N-C SACs were obtained with rod shape and highly oriented mesopores inherited. The XAS spectrum revealed the electronic and structural information of the Fe-N-C SACs. Moreover, this kind of SACs possesses outstanding ORR activity in both alkaline and acidic media, better than most reported non-noble metal catalysts. Gong *et al.* proposed a general host-guest cooperative

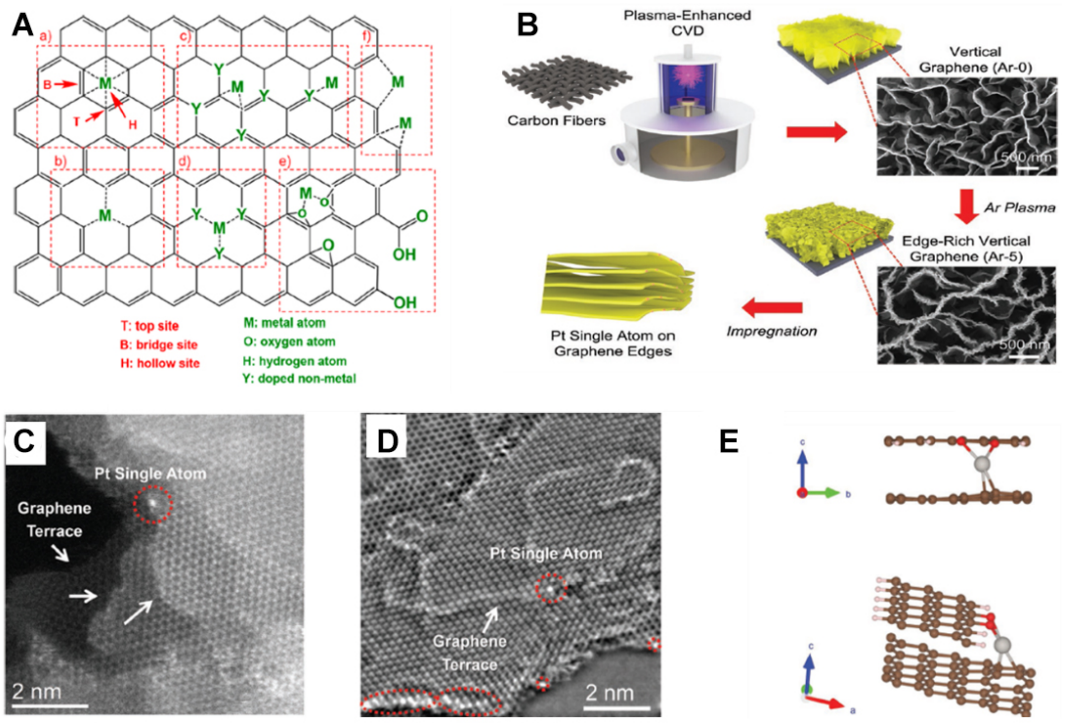

Figure 8. (A) Various binding modes of graphene-based SACs. (a) Supported on pristine graphene, (b) embedded on defective site with covalent metal-support Interaction (CMSIs), (c-e) supported or embedded on decorated graphene with CMSIs, and (f) adsorbed on the edge sites of graphene with CMSI. Reproduced from Ref.[109] with permission from the American Chemical Society. (B) Synthesis of the Pt Single Atoms on Graphene Edges with SEM Images of VG Ar-0 and VG Ar-5; (C and D) Ultra-high-resolution STEM of Pt SAC; (E) Optimized DFT structure based on structural characterizations. Reproduced from Ref.[111] with permission from Wiley-ACH.

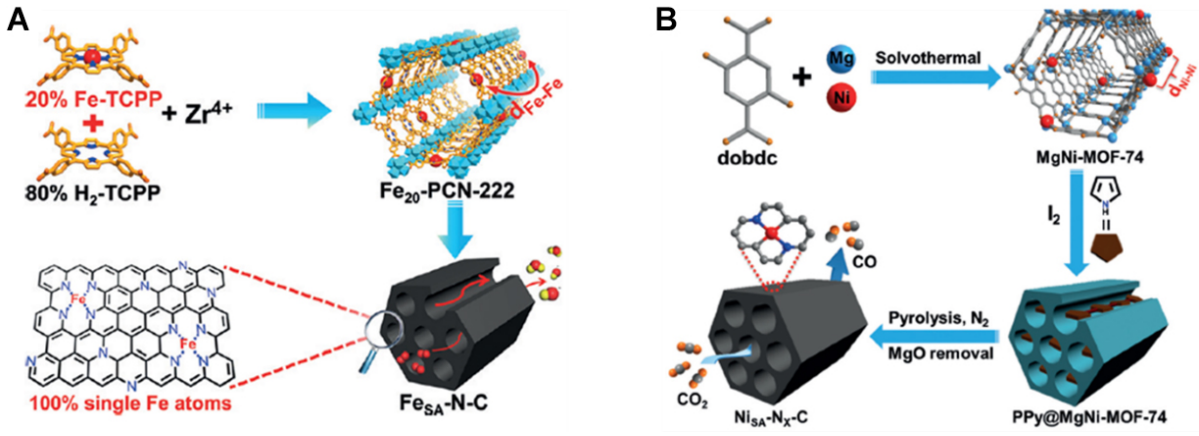

Figure 9. (A) Illustration of the synthesis of Fe SACs via a MOF-based mixed-ligand strategy. Reproduced from Ref.[114] with permission from Wiley-ACH. (B) Illustration of the host-guest cooperative protection strategy for the fabrication of NiSA-N_x-C catalysts for electrocatalytic CO_2 reduction. Reproduced from Ref.[115] with permission from Wiley-ACH.

protection strategy to fabricate a series of single-atom Ni catalysts (Ni_{SA}-N_x-C) by introducing polypyrrole (PPy) into MOF, as shown in Figure 9B[115]. HAADF-STEM images confirmed the good dispersion of the isolated Ni atoms. Encouraged by the single-atom structure, electrocatalytic CO_2 reduction was investigated to evaluate the catalyst performance. As expected, the Ni_{SA}-N_x-C affords a nearly 98% faradaic efficiency (FE) for CO formation.

Carbon black

Amorphous carbon or cheap carbon black is the most suitable substrate for practical application due to its economy and tractability. Generally, in order to anchor a single atom on the amorphous carbon tightly, many defects or heteroatoms should be created on the substrate[39,116-118]. Liu *et al.* proposed a series of carbon-defect-anchored Pt SACs using cost-effective carbon black and N-doped carbon black as substrates, respectively. For example, carbon black, urea, and chloroplatinic acid were mixed together, followed by high-temperature pyrolysis to obtain carbon-supported doped-N triggered Pt SAC (Pt_1-N/BP)[118]. The HAADF-STEM examination of multiple regions indicated that only isolated Pt atoms exist in the Pt_1-N/BP SACs. Further, the N 1s X-ray photoelectron spectroscopy (XPS) showed there exist five different types of N and obviously Pt-N bonding configuration. XAFS can also prove that Pt_1-N/BP contains only single Pt atoms, and doped-N can prohibit the oxidation of single Pt atoms, as shown in Figure 10A-F. And the electrochemical test indicated that the Pt_1-N/BP SACs are a highly efficient and stable electrocatalyst for the ORR. Liu *et al.* reported SACs in 2D carbon material with nanometer holes by bottom-up method, as shown in Figure 10G[117]. The key step is synthesizing a holey carbon skeleton network, as shown in Figure 10H. Volatile metal precursors are then added before heating to incorporate metal atoms in the carbon matrix. In the heat treatment under 300 °C and an inert gas atmosphere, the coordinated metal ion was reduced to an isolated single atom through the carbonization of the organic linker, thereby obtaining the SACs with defected-carbon as substrate. They used Ir SACs as an example, and no Ir atom aggregations were detected even at low resolution by the aberration-corrected (AC)-HAADF-STEM [Figure 10I-K]. At present, it is rare to use pure carbon as a substrate to fabricate SACs as a result of weak interaction between the metal and substrate, easily leading to aggregation of metal during the synthesis and operation process.

TYPICAL APPLICATIONS OF SACS

The SACs have been applied to various energy-related reactions due to their excellent activity, metal utilization, and selectivity. Especially O_2, CO_2 and N_2 reduction, as well as H_2 evolution, *etc.*, highly rely on precious metals.

O_2 reduction reaction

Oxygen reduction reaction (ORR) is an important half-cell for proton-exchange membrane fuel cells (PEMFCs), anion-exchange membrane fuel cells (AEMFCs), and metal-air batteries[119-122]. At present, the state-of-the-art electrocatalyst for ORR is platinum group metals (PGMs), which benefit from their promising activity and stability. However, due to their scarcity and high costs, how to reduce the dosage of PGM and maintain the required performance is highly demanded. SACs for ORR, including precious metal-based and nonprecious metal-based, usually have active metal centers (M = Pt, Mn, Fe, Co, *etc.*) coordinated to nitrogen on a conductive substrate, which shows outstanding ORR activity[123]. Liu fabricated Pt SACs anchored by carbon defects, or N species, which showed remarkable ORR activity and durability, typically making Pt utilization up to 0.09 g_{Pt} kW^{-1}[39,118]. Li *et al.* proposed a kind of PGM-free SACs for ORR in PEMFC with FeN_4 species embedded in partially graphitized carbon by a controlled thermal activation separating the formation of active species from carbonization and nitrogen-doping process as shown in Figure 11A[124]. The optimized catalyst showed remarkable catalytic performance for the ORR with $E_{1/2}$ up to 0.81 V in acid conditions and generated a current density of about 0.03 A (at 0.9 $V_{IR\text{-}free}$) approaching the DOE target (0.044 A cm^{-2}), as shown in Figure 11B and C. Li synthesized atomically dispersed Zn-N-C SACs for the ORR with an ultrahigh Zn loading of 9.33 wt.% by controlling the annealing rate at 1 min^{-1}[125]. HAADF-STEM image clearly indicated that single Zn atoms were well dispersed in the Zn-N-C catalyst at a high density [Figure 11D and E]. The optimized catalyst reached a half-wave potential of 0.746 V in acidic media and 0.874 V in alkaline conditions, in which the ORR properties in alkaline media were higher than that of the commercial catalyst Pt/C (0.858 V), as shown in Figure 11F and G. And the Zn-N-C SACs also showed acceptable stability in acidic media and excellent durability in alkaline media with almost no

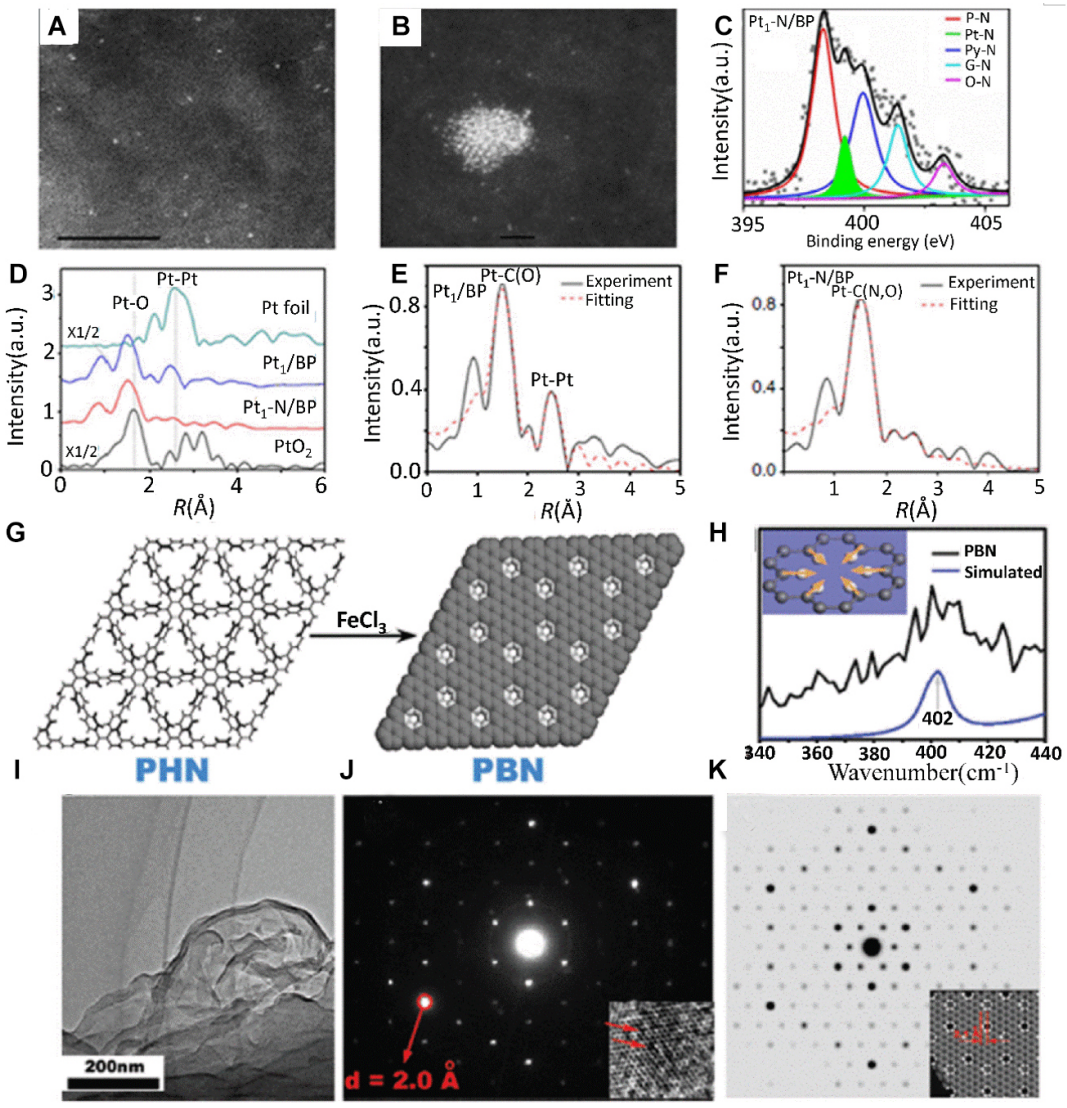

Figure 10. HAADF-STEM images of Pt_1-N/BP (A) and Pt_1/BP without N-doped (B); corresponding scale bar, 5 nm (A) and 1 nm (B); (C) XPS spectra for N 1s in Pt_1-N/BP; (D) The k^2-weighted R-space FT spectra from EXAFS, EXAFS fitting in R-space for (E) Pt_1/BP without N-doped; (F) Pt_1-N/BP. Reproduced from Ref.[118] with permission from Springer Nature. The characterizations of the nanometer hole defect on PBN; (G) The reaction scheme to prepare PBN; (H) Raman spectrum; (I) TEM image; (J) HRTEM image with SAED spectrum (inset); (K) Layered offset stacking structure of PBN with holes on top of hexabenzocoronene cores. Reproduced from Ref.[117] with permission from Wiley-ACH.

obvious change in half-wave potential after 1,000-cycle test. The excellent stability of SACs can be attributed to their typical structure, in which strong metal-support interactions play an important role in stabilizing the SACs. The XPS analysis and DFT calculations indicate that the Zn-N-C catalyst was less susceptible to protonation in an acidic solution and thus had good durability. Besides, an amount of M-N-C (M = Ir, Pd, Co, Mn) SACs have been developed for the ORR[26,126-131]. Despite the great achievements that have been achieved in recent years, there remain great challenges for the practical industry of PGM-free SACs. One is how to control the SACs structure during the synthesis process precisely. The other is how to improve the performance and durability of SACs.

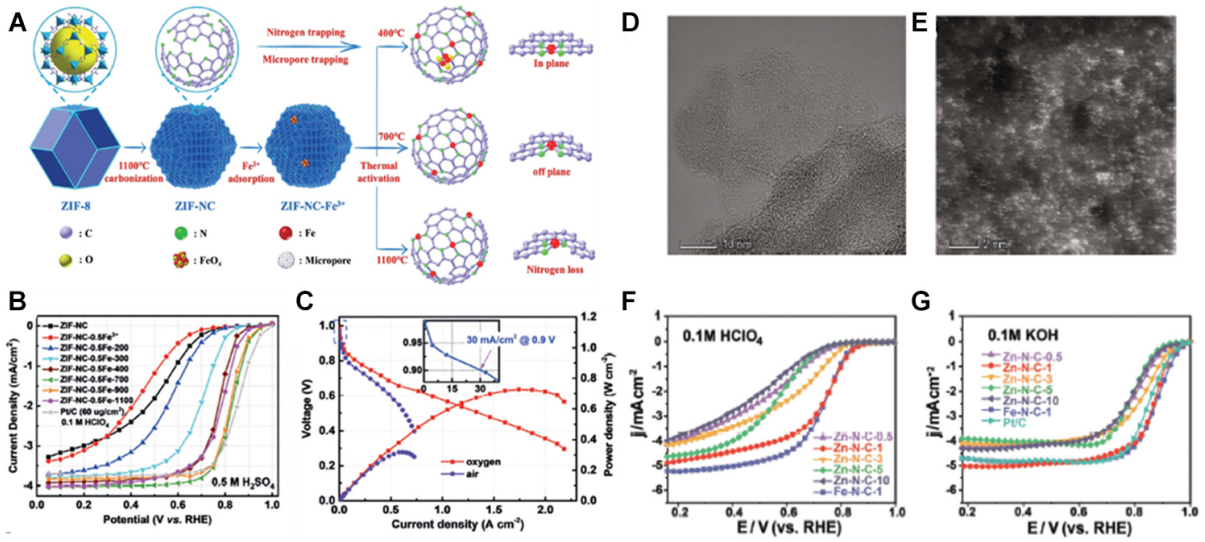

Figure 11. (A) Schematic Fe SACs fabrication process by adsorbing Fe into N-doped carbon; no complex carbonization and nitrogen-doping processes occurred during thermal activation; (B) ORR polarization plots in 0.5 M H_2SO_4 electrolyte; (C) Fuel cell performance of the best-performing Fe SAC under both H_2/O_2 and H_2/air conditions. Reproduced from Ref.[124] with permission from Wiley-ACH. (D) Aberration-corrected HAADF-STEM image of the Zn-NC-1 catalyst; (E) HRTEM image of the Zn-NC-1 catalyst; ORR polarization curves of Zn-N-C-X and Fe-N-C-X catalysts recorded in O_2-saturated 0.1 M $HClO_4$ (F) and 0.1 M KOH solution (G); Reproduced from Ref.[125] with permission from Wiley-ACH.

CO_2 reduction reaction

Electrochemical reduction of carbon dioxide (CO_2RR) to value-added chemicals is a promising approach to using CO_2 more efficiently and environmentally friendly. Over the last few decades, a variety of metal electrocatalysts have been explored, in which transition metals, such as Au, Ag, and Cu, are typically active for the reduction of CO_2 to CO or multi-carbon materials[132-135]. Compared to metallic electrodes or other electrocatalysts, SACs with cationic metal centers used for CO_2RR have obvious advantages, such as high utilization of the active sites and the ability to stabilize reaction intermediates and restrict the structure of adsorbates, leading to improvement of catalyst activity and selectivity. Mou constructed a highly efficient Ni-based SAC for CO_2RR via an impregnation-pyrolysis method, as shown in Figure 12A-E[136]. And XAFS, as well as HAADF-STEM, confirmed the presence of single Ni atoms. And an outstanding CO FE of up to 90.2% was achieved when the Ni SACs were applied to the CO_2RR. Further, DFT calculations indicated that the remarkable activities came from coordinatively unsaturated Ni-N sites since the free energies for the formation of intermediate *COOH on Ni-N sites are much lower than that on Ni-N_4 sites. Although plenty of SACs have been synthesized for CO_2RR, the evolution of active sites during the fabrication and operation process is still a hot issue. Yan obtained Cu SACs with Cu embedded in N-doped porous carbon via the pyrolysis of Cu-doped ZIF-8, which shows a high CO Faradaic efficiency of 93.5%[137]. They also studied the evolution of Cu SACs during the CO_2RR process carefully. It is obviously observed that the isolated Cu single atom converted nanoclusters recorded by HADDF-STEM [Figure 12F-I]. DFT calculation indicated that the higher reactivity of metallic Cu sites, especially nanoclusters, enhances the CO_2 conversion to CO. Many problems remain about the mechanisms of SACs in CO_2RR. It is highly urgent to elucidate the difference in catalyst mechanisms between different kinds of SACs and the evolution of active sites during the CO_2RR process[138,139].

N_2 reduction

Electrochemical Nitrogen reduction reaction (NRR) is a promising method to replace the traditional Haber-bosch process for artificial N_2 fixation[140-142]. Usually, a six-electron process was involved in producing

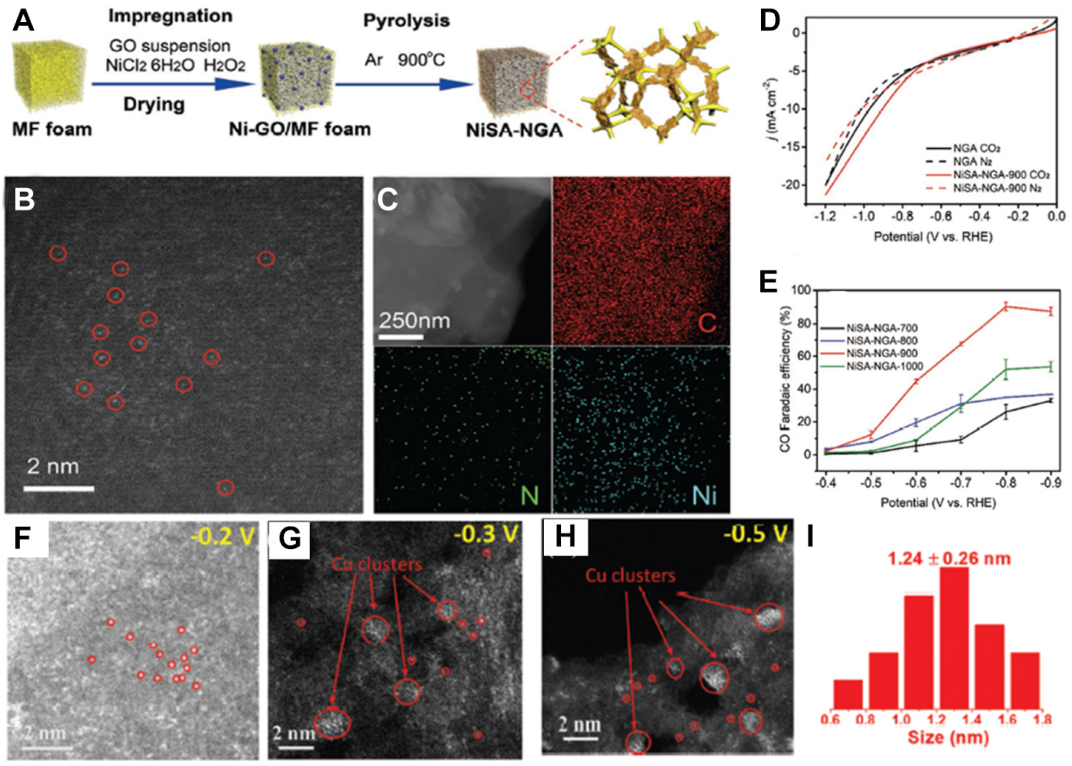

Figure 12. (A) Schematic illustration of the synthesis of N SACs; (B) HAADF-STEM image of NiSA-NGA; (C) STEM images and the corresponding EDS elemental maps of C, N, and Ni for NiSA-NGA; (D) LSV curves of NiSA-NGA catalysts in CO_2-saturated and N_2-saturated 0.5 m $KHCO_3$ electrolyte; (E) CO Faradaic efficiency. Reproduced from Ref.[136] with permission from Wiley-ACH. (F-H) HADDF-STEM images of CuNC-DCD after the CO_2RR test for 30 min at (F) -0.20 V, (G) -0.30 V, and (H) -0.50 V; (I) Size histograms of Cu nanoclusters from CuNC-DCD after the CO_2RR test at -0.50 V for 30 min; Reproduced from Ref.[137] with permission from the Royal Society of Chemistry.

ammonia molecules, and a side reaction with a four-electron process to give hydrazine was difficult to be avoided. At present, a variety of catalysts have been developed to improve the yield rate of ammonia. Typically, SACs have been paid a lot of attention due to their advantage[15,143,144]. Yu proposed a strategy to synthesize Ru SACs (Ru SAs/g-C_3N_4) with single Ru atoms distributed in bulk graphitic carbon nitride[145]. HADDF-STEM image demonstrated the well-dispersed Ru single atoms on the substrate. The catalytic activity and selectivity under ambient conditions have been evaluated and compared with bulk Ru surfaces. High catalytic activity and selectivity in NRR were achieved with an NH_3 yield rate of 23.0 μg mg $cat^{-1}h^{-1}$ and an NH_3 FE of 8.3 %, which is much better than that of bulk Ru catalyst, as shown in Figure 13. Moreover, high stability was observed by five recycling tests and a 12 h potentiostatic test. The DFT calculation proved that the H poisoning effect is much less significant at this kind of Ru SAs/g-C_3N_4, causing high selectivity for the NRR. Besides, many other metal-nitrogen-carbon(M-N-C) materials showed remarkable activities for electrochemical NRR synthesis. However, the NRR is still in its infancy, with many questions needed to be answered. It is still a big challenge to clarify the active sites. He *et al.* used iron phthalocyanine (FePc) with well-defined FeN_4 sites and N sites, as well as Pc without Fe center, as model catalysts to investigate the true active sites in Fe-NC catalysts for electrochemical NRR[16]. The experiments and DFT calculation indicate that the electrocatalytic NRR prefers to take place on the Fe site of the FeN_4 configuration of FePc via a preferred alternating pathway. This well-defined M-NC material with FePc loaded on the porous carbon showed a high NH_3 yield rate of 137.95 μg $mg_{FePc}cat^{-1}h^{-1}$ at a low potential of -0.3 V. Up to now, the development of NRR is still far from industrial application. Besides the identity of active sites, the activation of inert N_2 molecules and the improvement of the yield and FE are also urgent issues.

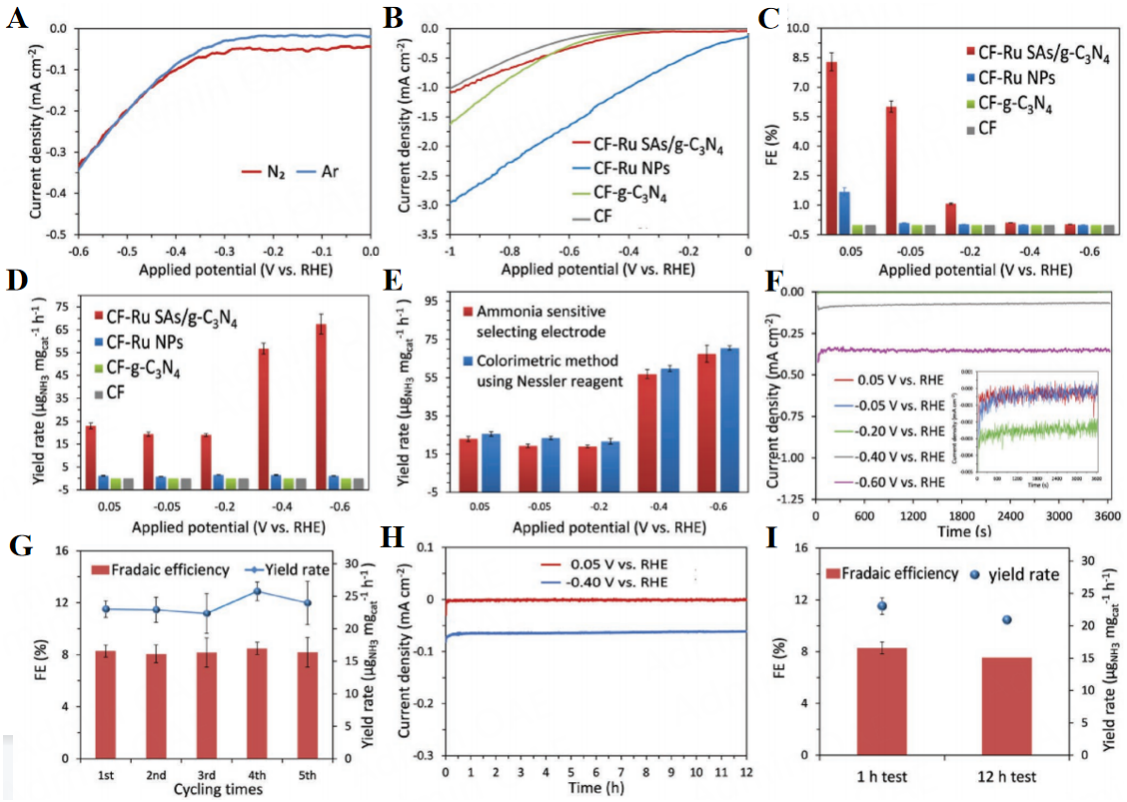

Figure 13. Electrochemical NRR performance; (A) LSV curves of Ru CF-SAs/g-C_3N_4 in a N_2 and Ar saturated 0.5 M NaOH aqueous solution; (B) LSV curves of CF, CF-g-C_3N_4, CF-Ru NPs, and CF-Ru SAs/g-C_3N_4 electrodes in a N_2 saturated aqueous solution of 0.5 M NaOH; (C) FEs and (D) ammonia yield rates at different potentials ranging from 0.05 to -0.60 V *vs.* RHE; (E) Comparison of the ammonia-sensitive selecting electrode and Nessler reagent-based colorimetric method for the quantitative analysis of ammonia yield rate; (F) Chronoamperometry results at the corresponding potentials; (G) FEs and ammonia yield rates during five consecutive cycles; (H) Chronoamperometry results at the 0.05 and -0.40 V *vs.* RHE; (I) FEs and ammonia yield rates within 1 and 12 h tests; Reproduced from Ref.[145] with permission from Wiley-ACH.

H_2 evolution

Hydrogen evolution reaction (HER) is a very important half-reaction for water splitting, which is highly desired for the hydrogen economy[146,147]. Normally, HER is a multistep electrochemical reaction process, highly dependent on the pH values of electrolytes[148-151]. Generally, Pt-based catalysts are still the most active catalysts and irreplaceable for the HER at present. However, the high cost limits their large-scale application. Ye *et al.* synthesized Pt SACs with single Pt atomic sites anchored on aniline-stacked graphene with Pt loading of 0.44 wt.%[152]. This kind of Pt SACs presents an outstanding HER activity with negligible onset potential and an overpotential around 12 mV at 10 mA cm^{-2} in 0.5 M H_2SO_4 solution, as shown in Figure 14A-F. And it also presents excellent stability with almost no current decay or structural changes during the durability test. The EXAFs confirmed the Pt single-atom structure and suggested a Pt site coordinates with four aniline molecules. Further DFT calculation indicated that the aniline molecules alter the electronic structure of Pt, which is responsible for the appropriate hydrogen adsorption energy for single Pt atoms. The SACs strategy maximizes the Pt utilization by effectively decreasing the precious metal loading and enhancing the mass activity. Recently, the development of non-noble-metal-based catalysts has been a promising alternative for HER. Pan *et al.* developed Fe-based SACs with atomically dispersed Fe-N_4 anchored on porous carbon by polymerization-pyrolysis evaporation strategy, as shown in Figure 14G and H[153]. The HAADF-STEM and X-ray spectroscopy (EDS) images suggest that the N and Fe species are distributed uniformly on the substrate. These Fe SACs showed a very small overpotential of

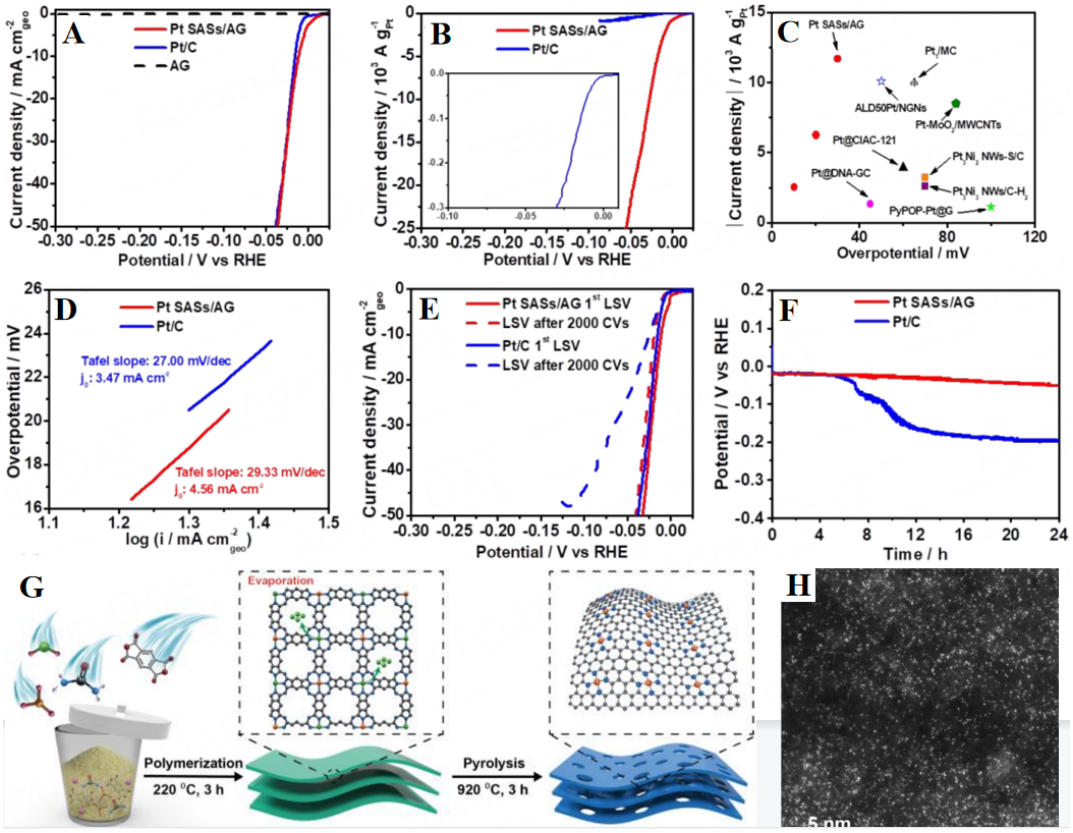

Figure 14. LSV curves of Pt SASs/AG and Pt/C with current density normalized to the (A) geometry area and (B) mass of Pt in 0.5 M H_2SO_4 at 2 mV s^{-1}; (C) Mass activities of Pt SASs/AG, Pt/C, and other state-of-the-art Pt-based catalysts in 0.5 M H_2SO_4; (D) Tafel plots of Pt SASs/AG and Pt/C; (E) LSV curves of Pt SASs/AG before and after 2,000 catalytic cycles; (F) Chronopotentiometric curves of Pt SASs/AG and Pt/C at 10 mA cm^{-2} in 0.5 M H_2SO_4 solution. Reproduced from Ref.[152] with permission from the Royal Society of Chemistry. (G) Synthesis scheme; (H) AC HAADF-STEM of the Fe SACs. Reproduced from Ref.[153] with permission from Wiley-ACH.

0.202 V at 10 mA cm^{-2}, with a Tafel slope of 123 mV dec^{-1} and a smaller charge-transfer resistance. Moreover, the Fe SACs had excellent stability with almost no change in morphology and distribution of elements after long-term electrolysis. In summary, SACs based on both noble and non-noble metals showed outstanding activity toward HER. The main challenge is that the loading of active metals remains relatively low for SACs, restricting further commercial application.

CH_4 conversion

Methane (CH_4), as the main component of natural gas, has been widely used for preparing value-added chemicals, especially C1 chemicals such as CH_3OH and HCOOH[37,154]. And it is a great challenge to obtain liquid oxygenates directly from CH_4 due to the requirement of extremely high activation energy and possible overoxidation under serious reaction conditions. SACs photocatalysts have shown great potential and become a very active research field in photocatalysis, benefiting from their enhancement of light harvesting, charge transfer capacity, and fast surface reactions. Wang reported low-cost tungsten single-atom photocatalysts synthesized by calcining the mixture of urea and sodium tungstate under the atmosphere[155]. A highly efficient CH_4 photooxidation process in water vapor under mild conditions was achieved as the single atom catalyst can manage H_2O_2 *in situ* generations and decomposition into OH radical. The HAADF-STEM image suggests that the well-dispersed W single atoms were successfully anchored onto the PCN substrate. Excellent catalyst activity and selectivity for CH_4 oxidation to C1 oxygenates were achieved with 4,956 μmol·g^{-1} cat yield and nearly 100% selectivity, as shown in

Figure 15A-C, better than most of the reported non-noble metal photocatalyst under mild conditions. Tang *et al.* synthesized Cu-based SACs with isolated Cu atoms onto the ZSM-5 support, where Cu_1-O_4 has been claimed as an active site[156]. Such Cu SACs showed high activity for direct CH_4 oxidation with C1 oxygenates productivity of 4,800 μmol·g^{-1} cat at 50 °C and 12,000 μmol·g^{-1} cat at 70 °C within 30 min, comparable to most of those state-of-the-art precious metal catalyst. Bai fabricated a cerium dioxide (CeO_2) nanowire supported Rh single atom (Rh-CeO_2 NWs SACs) for CH_4 conversion to oxygenates under mild conditions[157]. AC-HAADF/STEM image and EXAFs confirm the single atom, as shown in Figure 15D-I. A low CO_X selectivity around 6.1 wt.% was obtained, suggesting the overoxidation of CH_4 is strongly restricted on this Rh-CeO_2 SA. Correspondingly, the yield of CH_3OH and CH_3OOH reach up to 940.3 and 291.4 mmol $g_{Rh}^{-1}h^{-1}$, respectively, which largely exceed the reported catalyst under the same conditions. Future more, it is still urgent to develop more highly efficient and selective SACs for CH_4 oxidation.

Other application

Besides the applications mentioned above, SACs have also been applied to many important energy-related reactions, such as oxygen evolution reaction (OER) and organic synthesis. The core of SACs is to develop SACs with controllable structures and properties, including high activity, stability, and selectivity.

CHALLENGES

High metal loading SACs

Although a large number of SACs have been synthesized and investigated carefully, the metal contents were generally lower than 1 wt.%, with exceptional exceeding 7 wt.%, much lower than the expected theoretical capacity of the substrates for anchoring metal atoms. In some reactions, low catalyst loading may increase the catalyst usage, thus resulting in the loss of mass transport and overperformance. So high-loading SACs have outstanding advantages in practical catalyst applications. It is a big challenge to improve the density of active metal sites due to the large surface free energy of single-atom metal. Up to now, there have been only a few effective strategies for SACs synthesis with high metal loading. Zhang applied a universal approach of electrochemical deposition to a wide range of metals and substrates for the synthesis of SACs. In this way, more than 30 different SACs were successfully fabricated from cathodic or anodic deposition by changing metal precursors and substrate[47]. Hai *et al.* introduced a versatile method by two-step pyrolysis combining impregnation to obtain SACs with ultra-high single-atom density up to 23 wt.% for 15 kinds of metal[158]. They proved that controlling the bonding of metal precursors with the substrate by stepwise ligand removal can restrict their thermally induced aggregation into nanoparticles. Xia *et al.* used graphene quantum dots interweaved into a carbon matrix as substrate, which provided numerous anchoring sites for single atoms to synthesize SACs with high transition-metal-atom loadings of up to 40 wt.%[159]. Zhou proposed a multilayer stabilization strategy for constructing M-SACs in heteroatom-doped graphitized carbon substrates (M = Fe, Co, Ru, Ir, and Pt), as shown in Figure 16[160]. A high metal loading up to 16 wt.% was achieved since the confinement by perfluorotetradecanoic acid (PFTA) bilayers, and polypyrrole (Ppy) layer can prevent single metal atoms from aggregating during the pyrolysis process. Increasing the density of single-atom metals while keeping them atomically dispersed well should be a promising method to further enhance the catalyst performance and practical application ability. In the future, more methods for the SACs with high metal loading are urgently needed to be explored.

Scale-up of SACs

At present, most of the SACs synthesis methods are usually complicated and time-consuming, thus unable to meet the requirement of large-scale fabrication. Therefore, it is highly required to develop facile and eco-friendly strategies for the large batch production of SACs at kilogram levels. Only a few methods have been validated for large-scale production of SACs. Gan *et al.* reported a straightforward and scalable ball milling method for the fabrication of Co-alloyed Pt (Pt_1/Co) SACs catalyst at kilogram levels. Gan proposed a

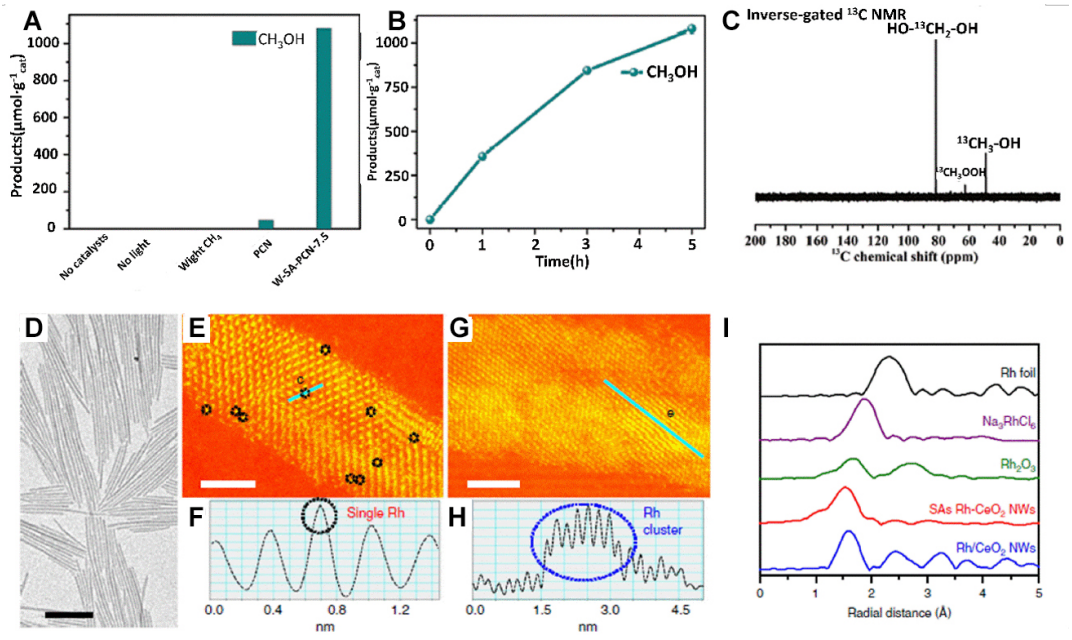

Figure 15. (A) CH_3OH yield of SAP and control samples; (B) Time-course plots of CHO_3OH yield. (C) Inverse-gated ^{13}C NMR spectra for $^{13}CH_4$ oxidation. Reproduced from Ref.[155] with permission from Wiley-ACH. Structural analyses of Rh-CeO_2 NWs SAs and Rh/CeO_2 NWs. (D) TEM image of the SAs Rh-CeO_2 NWs; (E) AC-HAADF/STEM image in temperature color of the SAs Rh-CeO_2 NWs; (F) The intensity profile recorded from the line in panel (E); (G) ACHAADF/STEM image in temperature color of the Rh/CeO_2 NWs; (H) The intensity profile recorded from the line in panel (G); (I) Rh K-edge EXAFS spectra in R space of the Rh foil, Na_3RhCl_6, Rh_2O_3, Rh-CeO_2 NWs SAs, and Rh/CeO_2 NWs; The scale bars in (D), (E), and (G) are 100, 2, and 2 nm, respectively. Reproduced from Ref.[157] with permission from Springer Nature.

scalable ball milling method for the synthesis of Co-alloyed Pt (Pt_1-Co) SACs at kilogram levels by the same synthesis route of a small level of Pt_1/Co just by increasing the amount of platinum precursor and cobalt precursor[161]. And the Pt-loading was identified to be 0.39 wt.% by the inductively coupled plasma-optical emission spectrometry (ICP-OES) technique. Gan *et al.* reported Au_1/CeO_2 SACs in large quantities (> 1 kg) by a dry ball-milling method with Au single atom loading of 0.1 wt.%[162]. proposed a method to generate Ru SACs on a kilogram scale with Ru loading of 0.3 wt% by mixing/calcination. Up to now, a few effective methods have been developed to fabricate high metal loading SACs at a large scale, which is very important progress for SACs, from bench-scale experiments to practical solutions for industrial productions.

CONCLUSION AND OUTLOOK

Single-atom electrocatalysis is a new frontier for energy-related research. Compared to conventional nanocatalysts based on nanoparticles or clusters, SACs with well-defined active sites usually show much better catalyst activity. SACs also have great potential for lowing the cost of energy-related electrochemical systems due to their high metal utilization efficiency. We summarized the synthetic methods, advanced characterization methods, and suitable substrates for SACs. We also discussed the typical application of SACs as well as the challenges. Nevertheless, although a large number of SACs have been reported in recent years, further development in the following aspects should be paid much attention to advancing the practical application: (1) revealing the reaction mechanism of SACs and understanding the relationship between SACs structure and properties for different applications; (2) improving the stability of SACs both in synthesis and operation process; (3) increasing the density of isolated single metals; and (4) developing more facial and time-saving synthesis strategy for scale-up production.

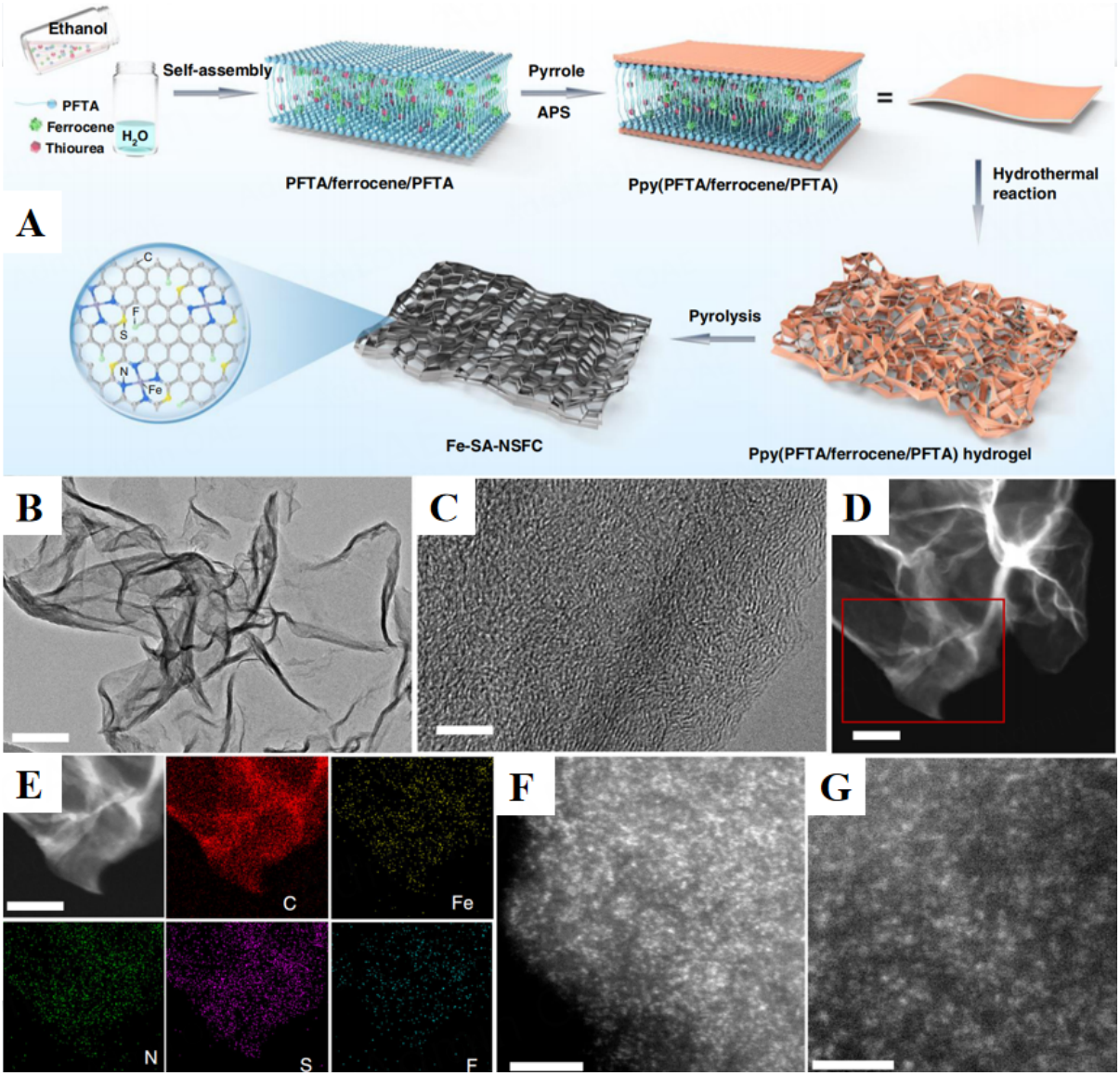

Figure 16. Synthesis and structural characterization results. (A) Illustration of the preparation process for the Fe-SA-NSFC and (B) TEM, (C) HRTEM, and (D) HAADF-STEM images of the Fe-SA-NSFC; (E) Enlarged HAADF-STEM image and corresponding element maps for C, Fe, N, S, and F. (F) AC-HAADF-STEM image and (G) high-magnification AC-HAADF-STEM image of the Fe-SA-NSFC. Scale bars: (B) 200 nm, (C) 5 nm, (D) 200 nm, (E) 100 nm, (F) 5 nm, and (G) 2 nm. Reproduced from Ref.[160] with permission from Springer Nature.

DECLARATIONS

Authors' contributions

Conceived the manuscript: Gong X, Xu W

Wrote and reviewed the manuscript: Gong X, Xu W

Contributed to the discussion of the manuscript: Gong X, Song P, Han C, Xiao Y, Mei X, Xu W

Availability of data and materials

Not applicable.

Financial support and sponsorship

This work was supported by the National Natural Science Foundation of China (22005294), the National Key R&D Program of China (2018YFB1502302, 2017YFE0197900), the National Science Foundation for Distinguished Young Scholars of China (21925205), and the National Natural Science Foundation of China (21733004, 21721003, 22072145).

Conflicts of interest

All authors declared that there are no conflicts of interest.

Ethical approval and consent to participate

Not applicable.

Consent for publication

Not applicable.

Copyright

© The Author(s) 2023.

REFERENCES

1. Wei YS, Zhang M, Zou R, Xu Q. Metal-organic framework-based catalysts with single metal sites. *Chem Rev* 2020;120:12089-174. DOI PubMed
2. Gao C, Low J, Long R, Kong T, Zhu J, Xiong Y. Heterogeneous single-atom photocatalysts: fundamentals and applications. *Chem Rev* 2020;120:12175-216. DOI PubMed
3. Ji Y, Liu S, Song S, et al. Negatively charged single-atom Pt catalyst shows superior SO_2 tolerance in NO_x reduction by CO. *ACS Catal* 2023;13:224-36. DOI
4. Yang M, Zhou K, Wang C, et al. Iridium single-atom catalyst coupled with lattice oxygen activated $CoNiO_2$ for accelerating the oxygen evolution reaction. *J Mater Chem A* 2022;10:25692-700. DOI
5. Kumar P, Al-Attas TA, Hu J, Kibria MG. Single atom catalysts for selective methane oxidation to oxygenates. *ACS Nano* 2022;16:8557-618. DOI PubMed
6. Ji S, Chen Y, Wang X, Zhang Z, Wang D, Li Y. Chemical synthesis of single atomic site catalysts. *Chem Rev* 2020;120:11900-55. DOI PubMed
7. Qiao B, Wang A, Yang X, et al. Single-atom catalysis of CO oxidation using Pt_1/FeO_x. *Nat Chem* 2011;3:634-41. DOI PubMed
8. Chen Y, He T, Liu Q, et al. Highly durable iron single-atom catalysts for low-temperature zinc-air batteries by electronic regulation of adjacent iron nanoclusters. *Appl Catal B Environ* 2023;323:122163. DOI
9. Wang S, Wang J. Single atom cobalt catalyst derived from co-pyrolysis of vitamin B_{12} and graphitic carbon nitride for PMS activation to degrade emerging pollutants. *Appl Catal B Environ* 2023;321:122051. DOI
10. Jin H, Cui P, Cao C, et al. Understanding the density-dependent activity of Cu single-atom catalyst in the benzene hydroxylation reaction. *ACS Catal* 2023;13:1316-25. DOI
11. Zhang X, Guo J, Guan P, et al. Catalytically active single-atom niobium in graphitic layers. *Nat Commun* 2013;4:1924. DOI PubMed
12. Zitolo A, Goellner V, Armel V, et al. Identification of catalytic sites for oxygen reduction in iron- and nitrogen-doped graphene materials. *Nat Mater* 2015;14:937-42. DOI PubMed
13. Jiang K, Siahrostami S, Zheng T, et al. Isolated Ni single atoms in graphene nanosheets for high-performance CO_2 reduction. *Energy Environ Sci* 2018;11:893-903. DOI
14. Zheng T, Jiang K, Ta N, et al. Large-scale and highly selective CO_2 electrocatalytic reduction on nickel single-atom catalyst. *Joule* 2019;3:265-78. DOI
15. Zhang R, Jiao L, Yang W, Wan G, Jiang H. Single-atom catalysts templated by metal-organic frameworks for electrochemical nitrogen reduction. *J Mater Chem A* 2019;7:26371-7. DOI
16. He C, Wu Z, Zhao L, et al. Identification of FeN_4 as an efficient active site for electrochemical N_2 reduction. *ACS Catal* 2019;9:7311-7. DOI
17. Fei H, Dong J, Arellano-Jiménez MJ, et al. Atomic cobalt on nitrogen-doped graphene for hydrogen generation. *Nat Commun* 2015;6:8668. DOI PubMed PMC
18. Shan J, Li M, Allard LF, Lee S, Flytzani-Stephanopoulos M. Mild oxidation of methane to methanol or acetic acid on supported isolated rhodium catalysts. *Nature* 2017;551:605-8. DOI PubMed
19. Lang R, Du X, Huang Y, et al. Single-atom catalysts based on the metal-oxide interaction. *Chem Rev* 2020;120:11986-2043. DOI

PubMed

20. Kaiser SK, Chen Z, Faust Akl D, Mitchell S, Pérez-Ramírez J. Single-atom catalysts across the periodic table. *Chem Rev* 2020;120:11703-809. DOI PubMed
21. Yang H, Shang L, Zhang Q, et al. A universal ligand mediated method for large scale synthesis of transition metal single atom catalysts. *Nat Commun* 2019;10:4585. DOI PubMed PMC
22. Wei H, Huang K, Wang D, et al. Iced photochemical reduction to synthesize atomically dispersed metals by suppressing nanocrystal growth. *Nat Commun* 2017;8:1490. DOI PubMed PMC
23. Ge X, Zhou P, Zhang Q, et al. Palladium single atoms on TiO_2 as a photocatalytic sensing platform for analyzing the organophosphorus pesticide chlorpyrifos. *Angew Chem Int Ed* 2020;59:232-6. DOI PubMed
24. Li Y, Hao J, Song H, et al. Selective light absorber-assisted single nickel atom catalysts for ambient sunlight-driven CO_2 methanation. *Nat Commun* 2019;10:2359. DOI PubMed PMC
25. Li H, Wang L, Dai Y, et al. Synergetic interaction between neighbouring platinum monomers in CO_2 hydrogenation. *Nat Nanotechnol* 2018;13:411-7. DOI PubMed
26. Yin P, Yao T, Wu Y, et al. Single cobalt atoms with precise N-coordination as superior oxygen reduction reaction catalysts. *Angew Chem Int Ed* 2016;55:10800-5. DOI PubMed
27. Ma R, Cui X, Wang Y, et al. Pyrolysis-free synthesis of single-atom cobalt catalysts for efficient oxygen reduction. *J Mater Chem A* 2022;10:5918-24. DOI
28. Yang HB, Hung S, Liu S, et al. Atomically dispersed Ni(i) as the active site for electrochemical CO_2 reduction. *Nat Energy* 2018;3:140-7. DOI
29. Chen Y, Ji S, Wang Y, et al. Isolated single iron atoms anchored on N-doped porous carbon as an efficient electrocatalyst for the oxygen reduction reaction. *Angew Chem Int Ed* 2017;56:6937-41. DOI PubMed
30. Wei S, Wang Y, Chen W, et al. Atomically dispersed Fe atoms anchored on COF-derived N-doped carbon nanospheres as efficient multi-functional catalysts. *Chem Sci* 2019;11:786-90. DOI PubMed PMC
31. Chen Y, Ji S, Sun W, et al. Engineering the atomic interface with single platinum atoms for enhanced photocatalytic hydrogen production. *Angew Chem Int Ed* 2020;59:1295-301. DOI PubMed
32. Yoo M, Yu Y, Ha H, et al. A tailored oxide interface creates dense Pt single-atom catalysts with high catalytic activity. *Energy Environ Sci* 2020;13:1231-9. DOI
33. Chen Y, Ji S, Zhao S, et al. Enhanced oxygen reduction with single-atomic-site iron catalysts for a zinc-air battery and hydrogen-air fuel cell. *Nat Commun* 2018;9:5422. DOI
34. Xiong Y, Dong J, Huang ZQ, et al. Single-atom Rh/N-doped carbon electrocatalyst for formic acid oxidation. *Nat Nanotechnol* 2020;15:390-7. DOI PubMed
35. Beniya A, Higashi S. Towards dense single-atom catalysts for future automotive applications. *Nat Catal* 2019;2:590-602. DOI
36. Riley C, Zhou S, Kunwar D, et al. Design of effective catalysts for selective alkyne hydrogenation by doping of ceria with a single-atom promotor. *J Am Chem Soc* 2018;140:12964-73. DOI PubMed
37. Kwon Y, Kim TY, Kwon G, Yi J, Lee H. Selective activation of methane on single-atom catalyst of rhodium dispersed on zirconia for direct conversion. *J Am Chem Soc* 2017;139:17694-9. DOI PubMed
38. Park J, Lee S, Kim HE, et al. Investigation of the support effect in atomically dispersed Pt on WO_{3-x} for utilization of Pt in the hydrogen evolution reaction. *Angew Chem Int Ed* 2019;58:16038-42. DOI
39. Liu J, Jiao M, Mei B, et al. Carbon-supported divacancy-anchored platinum single-atom electrocatalysts with superhigh Pt utilization for the oxygen reduction reaction. *Angew Chem Int Ed* 2019;58:1163-7. DOI PubMed
40. Fan L, Liu PF, Yan X, et al. Atomically isolated nickel species anchored on graphitized carbon for efficient hydrogen evolution electrocatalysis. *Nat Commun* 2016;7:10667. DOI PubMed PMC
41. Zhang L, Fischer JMTA, Jia Y, et al. Coordination of atomic Co-Pt coupling species at carbon defects as active sites for oxygen reduction reaction. *J Am Chem Soc* 2018;140:10757-63. DOI PubMed
42. Zhang L, Jia Y, Liu H, et al. Charge polarization from atomic metals on adjacent graphitic layers for enhancing the hydrogen evolution reaction. *Angew Chem Int Ed* 2019;58:9404-8. DOI PubMed
43. Shi Y, Huang WM, Li J, et al. Site-specific electrodeposition enables self-terminating growth of atomically dispersed metal catalysts. *Nat Commun* 2020;11:4558. DOI PubMed PMC
44. Li R, Li Y, Yang P, et al. Electrodeposition: synthesis of advanced transition metal-based catalyst for hydrogen production via electrolysis of water. *J Energy Chem* 2021;57:547-66. DOI
45. Tavakkoli M, Holmberg N, Kronberg R, et al. Electrochemical activation of single-walled carbon nanotubes with pseudo-atomic-scale platinum for the hydrogen evolution reaction. *ACS Catal* 2017;7:3121-30. DOI
46. Zhang L, Han L, Liu H, Liu X, Luo J. Potential-cycling synthesis of single platinum atoms for efficient hydrogen evolution in neutral media. *Angew Chem Int Ed* 2017;56:13694-8. DOI PubMed PMC
47. Zhang Z, Feng C, Liu C, et al. Electrochemical deposition as a universal route for fabricating single-atom catalysts. *Nat Commun* 2020;11:1215. DOI PubMed PMC
48. Han Y, Wang YG, Chen W, et al. Hollow N-doped carbon spheres with isolated cobalt single atomic sites: superior electrocatalysts for oxygen reduction. *J Am Chem Soc* 2017;139:17269-72. DOI PubMed
49. Sun T, Zhao S, Chen W, et al. Single-atomic cobalt sites embedded in hierarchically ordered porous nitrogen-doped carbon as a

superior bifunctional electrocatalyst. *Proc Natl Acad Sci USA* 2018;115:12692-7. DOI PubMed PMC

50. Rao P, Wu D, Qin Y, et al. Facile fabrication of single-atom catalysts by a plasma-etching strategy for oxygen reduction reaction. *J Mater Chem A* 2022;10:6531-7. DOI
51. Qiu HJ, Ito Y, Cong W, et al. Nanoporous graphene with single-atom nickel dopants: an efficient and stable catalyst for electrochemical hydrogen production. *Angew Chem Int Ed* 2015;54:14031-5. DOI PubMed
52. Wang B, Wang X, Zou J, et al. Simple-cubic carbon frameworks with atomically dispersed iron dopants toward high-efficiency oxygen reduction. *Nano Lett* 2017;17:2003-9. DOI PubMed
53. Li A, Kan E, Chen S, et al. Enabling high loading in single-atom catalysts on bare substrate with chemical scissors by saturating the anchoring sites. *Small* 2022;18:e2200073. DOI PubMed
54. Kim YH, Heo JS, Kim TH, et al. Flexible metal-oxide devices made by room-temperature photochemical activation of sol-gel films. *Nature* 2012;489:128-32. DOI PubMed
55. Liu P, Zhao Y, Qin R, et al. Photochemical route for synthesizing atomically dispersed palladium catalysts. *Science* 2016;352:797-800. DOI PubMed
56. Li T, Liu J, Song Y, Wang F. Photochemical solid-phase synthesis of platinum single atoms on nitrogen-doped carbon with high loading as bifunctional catalysts for hydrogen evolution and oxygen reduction reactions. *ACS Catal* 2018;8:8450-8. DOI
57. Zhou J, Duo F, Jia C, Zhou Y, Wang C, Wei Z. Photochemical solid-phase *in situ* anchoring of single atoms Ag/g-C_3N_4 for enhanced photocatalytic activity. *Environ Eng Sci* 2021;38:1098-107. DOI
58. Lu X, Guo C, Zhang M, et al. Rational design of palladium single-atoms and clusters supported on silicoaluminophosphate-31 by a photochemical route for chemoselective hydrodeoxygenation of vanillin. *Nano Res* 2021;14:4347-55. DOI
59. Fonseca J, Lu J. Single-atom catalysts designed and prepared by the atomic layer deposition technique. *ACS Catal* 2021;11:7018-59. DOI
60. Liu L, Corma A. Confining isolated atoms and clusters in crystalline porous materials for catalysis. *Nat Rev Mater* 2021;6:244-63. DOI
61. Cheng N, Stambula S, Wang D, et al. Platinum single-atom and cluster catalysis of the hydrogen evolution reaction. *Nat Commun* 2016;7:13638. DOI PubMed PMC
62. Parsons GN, Clark RD. Area-selective deposition: fundamentals, applications, and future outlook. *Chem Mater* 2020;32:4920-53. DOI
63. Cao K, Cai J, Chen R. Inherently selective atomic layer deposition and applications. *Chem Mater* 2020;32:2195-207. DOI
64. Zhang L, Banis MN, Sun X. Single-atom catalysts by the atomic layer deposition technique. *Natl Sci Rev* 2018;5:628-30. DOI
65. Cao L, Liu W, Luo Q, et al. Atomically dispersed iron hydroxide anchored on Pt for preferential oxidation of CO in H_2. *Nature* 2019;565:631-5. DOI PubMed
66. Wang X, Jin B, Jin Y, Wu T, Ma L, Liang X. Supported single Fe atoms prepared via atomic layer deposition for catalytic reactions. *ACS Appl Nano Mater* 2020;3:2867-74. DOI
67. Fei H, Dong J, Wan C, et al. Microwave-assisted rapid synthesis of graphene-supported single atomic metals. *Adv Mater* 2018;30:e1802146. DOI PubMed
68. Ding S, Guo Y, Hülsey MJ, et al. Electrostatic stabilization of single-atom catalysts by ionic liquids. *Chem* 2019;5:3207-19. DOI
69. Cai M, Wu Z, Li Z, et al. Greenhouse-inspired supra-photothermal CO_2 catalysis. *Nat Energy* 2021;6:807-14. DOI
70. Wang F, Chen H, Sun X, et al. Single atom Fe in favor of carbon disulfide (CS_2) adsorption and thus the removal efficiency. *Sep Purif Technol* 2021;258:118086. DOI
71. Tieu P, Yan X, Xu M, Christopher P, Pan X. Directly probing the local coordination, charge state, and stability of single atom catalysts by advanced electron microscopy: a review. *Small* 2021;17:e2006482. DOI PubMed
72. Schilling AC, Groden K, Simonovis JP, et al. Accelerated Cu_2O reduction by single Pt atoms at the metal-oxide interface. *ACS Catal* 2020;10:4215-26. DOI
73. Lovejoy TC, Ramasse QM, Falke M, et al. Single atom identification by energy dispersive X-ray spectroscopy. *Appl Phys Lett* 2012;100:154101. DOI
74. Zhang J, Wu X, Cheong WC, et al. Cation vacancy stabilization of single-atomic-site $Pt_1/Ni(OH)_x$ catalyst for diboration of alkynes and alkenes. *Nat Commun* 2018;9:1002. DOI
75. Kraushofer F, Resch N, Eder M, et al. Surface reduction state determines stabilization and incorporation of Rh on α-Fe_2O_3 ($11\bar{2}02$). *Adv Mater Interfaces* 2021;8:2001908. DOI
76. Patel DA, Hannagan RT, Kress PL, Schilling AC, Çınar V, Sykes ECH. Atomic-scale surface structure and CO tolerance of NiCu single-atom alloys. *J Phys Chem C* 2019;123:28142-7. DOI
77. Xu J, Li X, Liu X, Liu J. EELS analysis of Ce valence state of SiO_2 supported CeO_2 nanoparticles, CeO_x nanoclusters and Ce single atoms. *Microsc Microanal* 2020;26:728-30. DOI
78. Pan X, Yan X, Dai S, Xu M, Graham G. Directly probing local coordination, charge state and stability of single atom catalysts. *Microsc Microanal* 2020;26:2468-9. DOI
79. Xu J, Wang Y, Wang D, Liu J. EELS analysis of two-dimensional Co_3O_4 and supported La single atoms. *Microsc Microanal* 2020;26:1762-3. DOI
80. Abbas I, Kim H, Shin C, Yoon S, Jung K. Differences in bifunctionality of ZnO and ZrO_2 in Cu/ZnO/ZrO_2/Al_2O_3 catalysts in hydrogenation of carbon oxides for methanol synthesis. *Appl Catal B Environ* 2019;258:117971. DOI

81. Bafaqeer A, Tahir M, Amin NAS. Synthesis of hierarchical ZnV_2O_6 nanosheets with enhanced activity and stability for visible light driven CO_2 reduction to solar fuels. *Appl Surf Sci* 2018;435:953-62. DOI
82. Cao L, Luo Q, Liu W, et al. Identification of single-atom active sites in carbon-based cobalt catalysts during electrocatalytic hydrogen evolution. *Nat Catal* 2019;2:134-41. DOI
83. Banholzer MJ, Millstone JE, Qin L, Mirkin CA. Rationally designed nanostructures for surface-enhanced Raman spectroscopy. *Chem Soc Rev* 2008;37:885-97. DOI PubMed PMC
84. Wei J, Qin SN, Yang J, et al. Probing single-atom catalysts and catalytic reaction processes by shell-isolated nanoparticle-enhanced raman spectroscopy. *Angew Chem Int Ed* 2021;60:9306-10. DOI PubMed
85. Niu S, Yang J, Qi H, et al. Single-atom Pt promoted Mo_2C for electrochemical hydrogen evolution reaction. *J Energy Chem* 2021;57:371-7. DOI
86. Bai J, Tamura M, Nakayama A, Nakagawa Y, Tomishige K. Comprehensive study on Ni- or Ir-based alloy catalysts in the hydrogenation of olefins and mechanistic insight. *ACS Catal* 2021;11:3293-309. DOI
87. Resasco J, Christopher P. Atomically dispersed Pt-group catalysts: reactivity, uniformity, structural evolution, and paths to increased functionality. *J Phys Chem Lett* 2020;11:10114-23. DOI PubMed
88. Parkinson GS, Novotny Z, Argentero G, et al. Carbon monoxide-induced adatom sintering in a Pd-Fe_3O_4 model catalyst. *Nat Mater* 2013;12:724-8. DOI PubMed
89. Marcinkowski MD, Yuk SF, Doudin N, et al. Low-temperature oxidation of methanol to formaldehyde on a model single-atom catalyst: Pd atoms on Fe_3O_4(001). *ACS Catal* 2019;9:10977-82. DOI
90. Liu K, Zhao X, Ren G, et al. Strong metal-support interaction promoted scalable production of thermally stable single-atom catalysts. *Nat Commun* 2020;11:1263. DOI PubMed PMC
91. Tao FF, Ma Z. Water-gas shift on gold catalysts: catalyst systems and fundamental studies. *Phys Chem Chem Phys* 2013;15:15260-70. DOI PubMed
92. Ding K, Gulec A, Johnson AM, et al. Identification of active sites in CO oxidation and water-gas shift over supported Pt catalysts. *Science* 2015;350:189-92. DOI PubMed
93. Spezzati G, Su Y, Hofmann JP, et al. Atomically dispersed Pd-O species on CeO_2(111) as highly active sites for low-temperature CO oxidation. *ACS Catal* 2017;7:6887-91. DOI
94. Zhang Z, Wu Q, Johnson G, et al. Generalized synthetic strategy for transition-metal-doped brookite-phase TiO_2 nanorods. *J Am Chem Soc* 2019;141:16548-52. DOI PubMed
95. Hoang S, Guo Y, Binder AJ, et al. Activating low-temperature diesel oxidation by single-atom Pt on TiO_2 nanowire array. *Nat Commun* 2020;11:1062. DOI
96. Shen Q, Cao C, Huang R, et al. Single chromium atoms supported on titanium dioxide nanoparticles for synergic catalytic methane conversion under mild conditions. *Angew Chem Int Ed* 2020;59:1216-9. DOI PubMed
97. Shen G, Zhang R, Pan L, et al. Regulating the spin state of Fe(III) by atomically anchoring on ultrathin titanium dioxide for efficient oxygen evolution electrocatalysis. *Angew Chem Int Ed* 2020;59:2313-7. DOI PubMed
98. Hu P, Amghouz Z, Huang Z, Xu F, Chen Y, Tang X. Surface-confined atomic silver centers catalyzing formaldehyde oxidation. *Environ Sci Technol* 2015;49:2384-90. DOI PubMed
99. Hu P, Huang Z, Amghouz Z, et al. Electronic metal-support interactions in single-atom catalysts. *Angew Chem Int Ed* 2014;53:3418-21. DOI
100. Chen Y, Kasama T, Huang Z, et al. Highly dense isolated metal atom catalytic sites: dynamic formation and *in situ* observations. *Chemistry* 2015;21:17397-402. DOI PubMed
101. Zhang S, Nguyen L, Liang JX, et al. Catalysis on singly dispersed bimetallic sites. *Nat Commun* 2015;6:7938. DOI PubMed
102. Nguyen L, Zhang S, Wang L, et al. Reduction of nitric oxide with hydrogen on catalysts of singly dispersed bimetallic sites Pt_1Co_m and Pd_1Co_n. *ACS Catal* 2016;6:840-50. DOI
103. Wang L, Zhang S, Zhu Y, et al. Catalysis and *in situ* studies of Rh_1/Co_3O_4 nanorods in reduction of NO with H_2. *ACS Catal* 2013;3:1011-9. DOI
104. Wang Q, Huang X, Zhao ZL, et al. Ultrahigh-loading of Ir single atoms on NiO matrix to dramatically enhance oxygen evolution reaction. *J Am Chem Soc* 2020;142:7425-33. DOI PubMed
105. Zhou X, Shen Q, Yuan K, et al. Unraveling charge state of supported Au single-atoms during CO oxidation. *J Am Chem Soc* 2018;140:554-7. DOI PubMed
106. Zhou X, Yang W, Chen Q, et al. Stable Pt single atoms and nanoclusters on ultrathin CuO film and their performances in CO oxidation. *J Phys Chem C* 2016;120:1709-15. DOI
107. Lang R, Li T, Matsumura D, et al. Hydroformylation of olefins by a rhodium single-atom catalyst with activity comparable to $RhCl(PPh_3)_3$. *Angew Chem Int Ed* 2016;55:16054-8. DOI
108. Yu WZ, Wang WW, Li SQ, et al. Construction of active site in a sintered copper-ceria nanorod catalyst. *J Am Chem Soc* 2019;141:17548-57. DOI PubMed
109. Zhuo HY, Zhang X, Liang JX, Yu Q, Xiao H, Li J. Theoretical understandings of graphene-based metal single-atom catalysts: stability and catalytic performance. *Chem Rev* 2020;120:12315-41. DOI PubMed
110. Zhang C, Sha J, Fei H, et al. Single-atomic ruthenium catalytic sites on nitrogen-doped graphene for oxygen reduction reaction in acidic medium. *ACS Nano* 2017;11:6930-41. DOI PubMed

111. Tsounis C, Subhash B, Kumar PV, et al. Pt single atom electrocatalysts at graphene edges for efficient alkaline hydrogen evolution. *Adv Funct Mater* 2022;32:2203067. DOI
112. Song Z, Zhang L, Doyle-davis K, Fu X, Luo J, Sun X. Recent advances in MOF-derived single atom catalysts for electrochemical applications. *Adv Energy Mater* 2020;10:2001561. DOI
113. Hu L, Li W, Wang L, Wang B. Turning metal-organic frameworks into efficient single-atom catalysts via pyrolysis with a focus on oxygen reduction reaction catalysts. *EnergyChem* 2021;3:100056. DOI
114. Jiao L, Wan G, Zhang R, Zhou H, Yu SH, Jiang HL. From metal-organic frameworks to single-atom fe implanted n-doped porous carbons: efficient oxygen reduction in both alkaline and acidic media. *Angew Chem Int Ed* 2018;57:8525-9. DOI PubMed
115. Gong YN, Jiao L, Qian Y, et al. Regulating the coordination environment of MOF-templated single-atom nickel electrocatalysts for boosting CO_2 reduction. *Angew Chem Int Ed* 2020;132:2727-31. DOI PubMed
116. Liu J, Bak J, Roh J, et al. Reconstructing the coordination environment of platinum single-atom active sites for boosting oxygen reduction reaction. *ACS Catal* 2021;11:466-75. DOI
117. Liu C, Pan G, Liang N, Hong S, Ma J, Liu Y. Ir single atom catalyst loaded on amorphous carbon materials with high HER activity. *Adv Sci* 2022;9:e2105392. DOI PubMed PMC
118. Liu J, Jiao M, Lu L, et al. High performance platinum single atom electrocatalyst for oxygen reduction reaction. *Nat Commun* 2017;8:15938. DOI
119. Zhao D, Shui JL, Grabstanowicz LR, et al. Highly efficient non-precious metal electrocatalysts prepared from one-pot synthesized zeolitic imidazolate frameworks. *Adv Mater* 2014;26:1093-7. DOI PubMed
120. Kattel S, Wang G. A density functional theory study of oxygen reduction reaction on Me-N_4 (Me = Fe, Co, or Ni) clusters between graphitic pores. *J Mater Chem A* 2013;1:10790. DOI
121. Holby EF, Wu G, Zelenay P, Taylor CD. Structure of Fe-N_x-C defects in oxygen reduction reaction catalysts from first-principles modeling. *J Phys Chem C* 2014;118:14388-93. DOI
122. Chen P, Zhou T, Xing L, et al. Atomically dispersed iron-nitrogen species as electrocatalysts for bifunctional oxygen evolution and reduction reactions. *Angew Chem Int Ed* 2017;56:610-4. DOI PubMed
123. Wang Y, Su H, He Y, et al. Advanced electrocatalysts with single-metal-atom active sites. *Chem Rev* 2020;120:12217-314. DOI PubMed
124. Li J, Zhang H, Samarakoon W, et al. Thermally driven structure and performance evolution of atomically dispersed FeN_4 Sites for oxygen reduction. *Angew Chem Int Ed* 2019;58:18971-80. DOI PubMed
125. Li J, Chen S, Yang N, et al. Ultrahigh-loading zinc single-atom catalyst for highly efficient oxygen reduction in both acidic and alkaline media. *Angew Chem Int Ed* 2019;58:7035-9. DOI PubMed
126. He F, Li K, Yin C, Wang Y, Tang H, Wu Z. Single Pd atoms supported by graphitic carbon nitride, a potential oxygen reduction reaction catalyst from theoretical perspective. *Carbon* 2017;114:619-27. DOI
127. Xiao M, Zhu J, Li G, et al. A single-atom iridium heterogeneous catalyst in oxygen reduction reaction. *Angew Chem Int Ed* 2019;58:9640-5. DOI PubMed
128. Wang C, Kim J, Tang J, et al. New strategies for novel MOF-derived carbon materials based on nanoarchitectures. *Chem* 2020;6:19-40. DOI
129. He Y, Hwang S, Cullen DA, et al. Highly active atomically dispersed CoN_4 fuel cell cathode catalysts derived from surfactant-assisted MOFs: carbon-shell confinement strategy. *Energy Environ Sci* 2019;12:250-60. DOI
130. Xiong X, Li Y, Jia Y, et al. Ultrathin atomic Mn-decorated formamide-converted N-doped carbon for efficient oxygen reduction reaction. *Nanoscale* 2019;11:15900-6. DOI PubMed
131. Yang Y, Mao K, Gao S, et al. O-, N-atoms-coordinated Mn Cofactors within a graphene framework as bioinspired oxygen reduction reaction electrocatalysts. *Adv Mater* 2018;30:e1801732. DOI PubMed
132. Guo Z, Cheng S, Cometto C, et al. Highly efficient and selective photocatalytic CO_2 reduction by iron and cobalt quaterpyridine complexes. *J Am Chem Soc* 2016;138:9413-6. DOI PubMed
133. Huan TN, Ranjbar N, Rousse G, et al. Electrochemical reduction of CO_2 catalyzed by Fe-N-C materials: a structure-selectivity study. *ACS Catal* 2017;7:1520-5. DOI
134. Jiao Y, Zheng Y, Chen P, Jaroniec M, Qiao SZ. Molecular scaffolding strategy with synergistic active centers to facilitate electrocatalytic CO_2 reduction to hydrocarbon/alcohol. *J Am Chem Soc* 2017;139:18093-100. DOI PubMed
135. Zhang Z, Xiao J, Chen XJ, et al. Reaction mechanisms of well-defined metal-N_4 sites in electrocatalytic CO_2 reduction. *Angew Chem Int Ed* 2018;57:16339-42. DOI
136. Mou K, Chen Z, Zhang X, et al. Highly efficient electroreduction of CO_2 on Nickel single-atom catalysts: atom trapping and nitrogen anchoring. *Small* 2019;15:e1903668. DOI PubMed
137. Yan L, Liang XD, Sun Y, et al. Evolution of Cu single atom catalysts to nanoclusters during CO_2 reduction to CO. *Chem Commun* 2022;58:2488-91. DOI PubMed
138. Varela AS, Ranjbar Sahraie N, Steinberg J, Ju W, Oh HS, Strasser P. Metal-doped nitrogenated carbon as an efficient catalyst for direct CO_2 electroreduction to CO and hydrocarbons. *Angew Chem Int Ed* 2015;54:10758-62. DOI PubMed
139. Hu X, Hval HH, Bjerglund ET, et al. Selective CO_2 reduction to CO in water using earth-abundant metal and nitrogen-doped carbon electrocatalysts. *ACS Catal* 2018;8:6255-64. DOI
140. Lü F, Zhao S, Guo R, et al. Nitrogen-coordinated single Fe sites for efficient electrocatalytic N_2 fixation in neutral media. *Nano*

Energy 2019;61:420-7. DOI

141. Liu Y, Xu Q, Fan X, et al. Electrochemical reduction of N_2 to ammonia on Co single atom embedded N-doped porous carbon under ambient conditions. *J Mater Chem A* 2019;7:26358-63. DOI
142. Qin Q, Heil T, Antonietti M, Oschatz M. Single-site gold catalysts on hierarchical N-doped porous noble carbon for enhanced electrochemical reduction of nitrogen. *Small Methods* 2018;2:1800202. DOI
143. Zheng J, Liao F, Wu S, et al. Efficient non-dissociative activation of dinitrogen to ammonia over lithium-promoted ruthenium nanoparticles at low pressure. *Angew Chem Int Ed* 2019;58:17335-41. DOI PubMed
144. Tao H, Choi C, Ding L, et al. Nitrogen fixation by Ru single-atom electrocatalytic reduction. *Chem* 2019;5:204-14. DOI
145. Yu B, Li H, White J, et al. Tuning the catalytic preference of ruthenium catalysts for nitrogen reduction by atomic dispersion. *Adv Funct Mater* 2020;30:1905665. DOI
146. Lu B, Guo L, Wu F, et al. Ruthenium atomically dispersed in carbon outperforms platinum toward hydrogen evolution in alkaline media. *Nat Commun* 2019;10:631. DOI PubMed PMC
147. Li X, Liu H, Chen Z, et al. Enhancing oxygen evolution efficiency of multiferroic oxides by spintronic and ferroelectric polarization regulation. *Nat Commun* 2019;10:1409. DOI PubMed PMC
148. Gobbi M, Bonacchi S, Lian JX, et al. Periodic potentials in hybrid van der Waals heterostructures formed by supramolecular lattices on graphene. *Nat Commun* 2017;8:14767. DOI PubMed PMC
149. Wang ZL, Hao XF, Jiang Z, et al. C and N Hybrid Coordination Derived Co-C-N complex as a highly efficient electrocatalyst for hydrogen evolution reaction. *J Am Chem Soc* 2015;137:15070-3. DOI PubMed
150. Deng J, Li H, Xiao J, et al. Triggering the electrocatalytic hydrogen evolution activity of the inert two-dimensional MoS_2 surface via single-atom metal doping. *Energy Environ Sci* 2015;8:1594-601. DOI
151. Ling C, Shi L, Ouyang Y, Zeng XC, Wang J. Nanosheet supported single-metal atom bifunctional catalyst for overall water splitting. *Nano Lett* 2017;17:5133-9. DOI PubMed
152. Ye S, Luo F, Zhang Q, et al. Highly stable single Pt atomic sites anchored on aniline-stacked graphene for hydrogen evolution reaction. *Energy Environ Sci* 2019;12:1000-7. DOI
153. Pan Y, Liu S, Sun K, et al. A bimetallic Zn/Fe polyphthalocyanine-derived single-atom Fe-N_4 catalytic site:a superior trifunctional catalyst for overall water splitting and Zn-air batteries. *Angew Chem Int Ed* 2018;57:8614-8. DOI
154. Lin J, Wang X. Rh single atom catalyst for direct conversion of methane to oxygenates. *Sci China Mater* 2018;61:758-60. DOI
155. Wang Y, Zhang J, Shi WX, et al. W single-atom catalyst for CH_4 photooxidation in water vapor. *Adv Mater* 2022;34:e2204448. DOI PubMed
156. Tang X, Wang L, Yang B, et al. Direct oxidation of methane to oxygenates on supported single Cu atom catalyst. *Appl Catal B Environ* 2021;285:119827. DOI
157. Bai S, Liu F, Huang B, et al. High-efficiency direct methane conversion to oxygenates on a cerium dioxide nanowires supported rhodium single-atom catalyst. *Nat Commun* 2020;11:954. DOI PubMed PMC
158. Hai X, Xi S, Mitchell S, et al. Scalable two-step annealing method for preparing ultra-high-density single-atom catalyst libraries. *Nat Nanotechnol* 2022;17:174-81. DOI
159. Xia C, Qiu Y, Xia Y, et al. General synthesis of single-atom catalysts with high metal loading using graphene quantum dots. *Nat Chem* 2021;13:887-94. DOI PubMed
160. Zhou Y, Tao X, Chen G, et al. Multilayer stabilization for fabricating high-loading single-atom catalysts. *Nat Commun* 2020;11:5892. DOI PubMed PMC
161. Gan T, Liu Y, He Q, Zhang H, He X, Ji H. Facile synthesis of kilogram-scale co-alloyed Pt single-atom catalysts via ball milling for hydrodeoxygenation of 5-hydroxymethylfurfural. *ACS Sustain Chem Eng* 2020;8:8692-9. DOI
162. Gan T, He Q, Zhang H, et al. Unveiling the kilogram-scale gold single-atom catalysts via ball milling for preferential oxidation of CO in excess hydrogen. *Chem Eng J* 2020;389:124490. DOI